

*Pacific
Journal of
Mathematics*

**QUANDLE THEORY AND THE OPTIMISTIC LIMITS OF
THE REPRESENTATIONS OF LINK GROUPS**

JINSEOK CHO

QUANDLE THEORY AND THE OPTIMISTIC LIMITS OF THE REPRESENTATIONS OF LINK GROUPS

JINSEOK CHO

For a given boundary-parabolic representation of a link group to $\mathrm{PSL}(2, \mathbb{C})$, Inoue and Kabaya suggested a combinatorial method to obtain the developing map of the representation using the octahedral triangulation and the shadow-coloring of certain quandles. A quandle is an algebraic system closely related to the Reidemeister moves, so their method changes quite naturally under the Reidemeister moves.

We apply their method to the potential function, which was used to define the optimistic limit, and construct a saddle point of the function. This construction works for any boundary-parabolic representation, and it shows that the octahedral triangulation is good enough to study all possible boundary-parabolic representations of the link group. Furthermore, the evaluation of the potential function at the saddle point becomes the complex volume of the representation, and this saddle point changes naturally under the Reidemeister moves because it is constructed using the quandle.

1. Introduction

A link L has the hyperbolic structure when there exists a discrete faithful representation $\rho : \pi_1(L) \rightarrow \mathrm{PSL}(2, \mathbb{C})$, where the *link group* $\pi_1(L)$ is the fundamental group of the link complement $\mathbb{S}^3 \setminus L$. The standard method to find the hyperbolic structure of L is to consider some triangulation of $\mathbb{S}^3 \setminus L$ and solve certain sets of equations. (These equations are called the *hyperbolicity equations*.) Each solution determines a boundary-parabolic representation¹ and one of them is the *geometric representation*, which means the determined boundary-parabolic representation is discrete and faithful. Due to Mostow's rigidity theorem, the hyperbolic structure of a link is a topological property. Therefore, it is natural to expect the invariance of the hyperbolic structure under the Reidemeister moves. However, this cannot be seen easily, because even a small change on the triangulation changes the solution radically.

MSC2010: primary 57M27; secondary 51M25, 58J28.

Keywords: optimistic limit, quandle, hyperbolic volume, boundary-parabolic representation, link group.

¹ *boundary-parabolic* means the image of the peripheral subgroup $\pi_1(\partial(\mathbb{S}^3 \setminus L))$ is a parabolic subgroup of $\mathrm{PSL}(2, \mathbb{C})$. Note that the geometric representation is boundary-parabolic.

Recently, Inoue and Kabaya [2014] developed a method to construct the hyperbolic structure of L using the link diagram and the geometric representation. More generally, for a given boundary-parabolic representation ρ , they constructed the explicit geometric shapes of the tetrahedra of certain triangulations using ρ . Their main method is to construct the geometric shapes using certain quandle homology, which is defined directly from the link diagram D and the representation ρ . Here, a quandle is an algebraic system whose axioms are closely related to the Reidemeister moves of link diagrams, so their construction changes quite naturally under the Reidemeister moves. (The definition of the quandle is in Section 2A. A good survey of quandles is the book [Elhamdadi and Nelson 2015].) A result of Inoue and Kabaya [2014] suggests a combinatorial method to obtain the hyperbolic structure of the link complement.

Interestingly, the triangulation used in [Inoue and Kabaya 2014] was also used to define the optimistic limit of the Kashaev invariant in [Cho et al. 2014]. As a matter of fact, this triangulation arises naturally from the link diagram. (See Section 3 of [Weeks 2005] and Section 2C of this article for the definition.) We call this triangulation *octahedral triangulation* of $\mathbb{S}^3 \setminus (L \cup \{\text{two points}\})$ associated with the link diagram D .

The optimistic limit first appeared in [Kashaev 1995] where the volume conjecture was proposed. This conjecture relates certain limits of link invariants, called Kashaev invariants, with the hyperbolic volumes. The optimistic limit, which was first defined in [Murakami 2000], is the value of a certain potential function evaluated at a saddle point, where the function and the value are expected to be an analytic continuation of the Kashaev invariant and the limit of the invariant, respectively. As a matter of fact, physicists usually call the evaluation the *classical limit* and consider it the *actual limit* of the invariant. A mathematically rigorous definition of the optimistic limit was proposed in [Yokota 2011] and the value was proved to coincide with the hyperbolic volume. Several versions of the optimistic limit have been developed, in a number of articles, but we will modify the version of [Cho et al. 2014] so as to construct a solution without the need to solve equations.

The optimistic limit is defined by the potential function $V(z_1, \dots, z_n, w_k^j, \dots)$. Previously, in [Cho et al. 2014], this function was defined purely by the link diagram, but here we modify it using the information of the representation ρ . (The definition is in Section 3.) We consider a solution of the set

$$\mathcal{H} := \left\{ \exp\left(z_k \frac{\partial V}{\partial z_k}\right) = 1, \exp\left(w_k^j \frac{\partial V}{\partial w_k^j}\right) = 1 \mid j : \text{degenerate crossings}, k = 1, \dots, n \right\},$$

which is a saddle-point of the potential function V . Then Proposition 3.1 will show that \mathcal{H} becomes the hyperbolicity equations of the octahedral triangulation.

Solving the equations in \mathcal{H} is not easy because there are infinitely many solutions.

The standard way to avoid this difficulty is to deform the octahedral triangulation of $\mathbb{S}^3 \setminus (L \cup \{\text{two points}\})$ to the triangulation of $\mathbb{S}^3 \setminus L$, as in [Yokota 2011]. However, this deformation produces the problem of the existence of solutions because some triangulations constructed from a link diagram may have no solution. (Sakuma and Yokota [2016] proved the existence of solutions for the alternating links.) Furthermore, the author believes these deformations of the triangulation lose the combinatorial properties of link diagrams. Therefore, we will use the octahedral triangulation without any deformation and do not solve the equations in \mathcal{H} . Instead, we will construct an explicit solution $(z_1^{(0)}, \dots, z_n^{(0)}, (w_k^j)^{(0)}, \dots)$ of \mathcal{H} .

Theorem 1.1. *Using the quandle associated with the representation ρ , there exists a formula to construct a solution $(z_1^{(0)}, \dots, z_n^{(0)}, (w_k^j)^{(0)}, \dots)$ of \mathcal{H} . (The exact formulas are in Theorem 3.2.)*

The evaluation of the potential function V depends on the choice of log-branch. To obtain a well-defined value, modify the potential function to

$$(1) \quad V_0(z_1, \dots, z_n, (w_k^j), \dots) := V(z_1, \dots, z_n, (w_k^j), \dots) - \sum_k \left(z_k \frac{\partial V}{\partial z_k} \right) \log z_k - \sum_{j,k} \left(w_k^j \frac{\partial V}{\partial w_k^j} \right) \log w_k^j.$$

Theorem 1.2. *For the constructed solution $(z_1^{(0)}, \dots, z_n^{(0)}, (w_k^j)^{(0)}, \dots)$ of \mathcal{H} and the modified potential function V_0 above, the following holds:*

$$(2) \quad V_0(z_1^{(0)}, \dots, z_n^{(0)}, (w_k^j)^{(0)}, \dots) \equiv i(\text{vol}(\rho) + i \text{cs}(\rho)) \pmod{\pi^2},$$

where $\text{vol}(\rho)$ and $\text{cs}(\rho)$ are the hyperbolic volume and the Chern–Simons invariant of ρ defined in [Zickert 2009], respectively.

The proof will be in Theorem 3.3. The left-hand side of (2) is called the *optimistic limit* of ρ , and $\text{vol}(\rho) + i \text{cs}(\rho)$ in the right-hand side is called *the complex volume* of ρ .

Note that for any boundary-parabolic representation ρ , we can always construct the solution associated with ρ . This implies that the octahedral triangulation is good enough for the study of all possible boundary-parabolic representations from the link group to $\text{PSL}(2, \mathbb{C})$. The set of all possible representations can be regarded as the *Ptolemy variety* (see [Garoufalidis et al. 2015] for detail) and we expect the octahedral triangulation will be very useful to the study of the Ptolemy variety. (An actual application to the Ptolemy variety is in preparation now.)

Furthermore, the construction of the solution is based on the quandle in [Inoue and Kabaya 2014]. Therefore, this solution changes locally under the Reidemeister moves. This implies that we can explore the hyperbolic structure of a link by finding the solution and keeping track of the changes of the solution under the Reidemeister

moves. As a matter of fact, after the appearance of the first draft of this article, this idea was successfully used in [Cho 2016a; Cho and Murakami 2017] and more applications are in preparation.

Among the applications, we remark that [Cho 2016a] contains very similar results to this article. Both articles construct the solution associated with ρ using the same quandle. However, the major differences are the triangulations. Both use the same *octahedral decomposition* of $\mathbb{S}^3 \setminus (L \cup \{\text{two points}\})$, but this article uses the subdivision of each octahedron into four tetrahedra and call the result *four-term (or octahedral) triangulation*, whereas [Cho 2016a] uses the subdivision of the same octahedron into five tetrahedra and calls the result *five-term triangulation*. Some tetrahedra in the four-term triangulation can be degenerate and this introduces technical difficulties. However, the five-term triangulation used in [Cho 2016a] does not contain any degenerate tetrahedra, so it is far easier and more convenient. In conclusion, this article contains the original idea of using a quandle to construct the solution and [Cho 2016a] improved the idea.

The layout of this article is as follows. In Section 2, we will summarize some results from [Inoue and Kabaya 2014]. In particular, the definition of the quandle and the octahedral triangulation will appear. Section 3 will define the optimistic limit and the hyperbolicity equations. The main formula (Theorem 3.3) of the solution associated with the given representation ρ will appear. Section 4 will discuss two simple examples, the figure-eight knot 4_1 and the trefoil knot 3_1 .

2. Quandles

In this section, we will survey some results of [Inoue and Kabaya 2014]. We remark that all formulas in this section come from that article, and the author learned them from the series of lectures given by Ayumu Inoue at Seoul National University during the spring of 2012.

2A. Conjugation quandle of parabolic elements.

Definition 2.1. A *quandle* is a set X with a binary operation $*$ satisfying the following three conditions:

- (1) $a * a = a$ for any $a \in X$.
- (2) The map $*b : X \rightarrow X$ ($a \mapsto a * b$) is bijective for any $b \in X$.
- (3) $(a * b) * c = (a * c) * (b * c)$ for any $a, b, c \in X$.

The inverse of $*b$ is notated by $*^{-1}b$. In other words, the equation $a *^{-1}b = c$ is equivalent to $c * b = a$.

Definition 2.2. Let G be a group and X be a subset of G satisfying

$$g^{-1}Xg = X \quad \text{for any } g \in G.$$

Define the binary operation $*$ on X by

$$(3) \quad a * b = b^{-1}ab$$

for any $a, b \in X$. Then $(X, *)$ becomes a quandle and is called the *conjugation quandle*.

As an example, let \mathcal{P} be the set of parabolic elements of $\text{PSL}(2, \mathbb{C}) = \text{Isom}^+(\mathbb{H}^3)$. Then,

$$g^{-1}\mathcal{P}g = \mathcal{P}$$

holds for any $g \in \text{PSL}(2, \mathbb{C})$. Therefore, $(\mathcal{P}, *)$ is a conjugation quandle, and this is the only quandle we use in this article.

To perform concrete calculations, an explicit expression of $(\mathcal{P}, *)$ was introduced in [Inoue and Kabaya 2014]. First, note that

$$\begin{pmatrix} p & q \\ r & s \end{pmatrix}^{-1} \begin{pmatrix} 1 & 1 \\ 0 & 1 \end{pmatrix} \begin{pmatrix} p & q \\ r & s \end{pmatrix} = \begin{pmatrix} 1+rs & s^2 \\ -r^2 & 1-rs \end{pmatrix},$$

for $\begin{pmatrix} p & q \\ r & s \end{pmatrix} \in \text{PSL}(2, \mathbb{C})$. Therefore, we can identify $(\mathbb{C}^2 \setminus \{0\})/\pm$ with \mathcal{P} by

$$(4) \quad (\alpha \ \beta) \longleftrightarrow \begin{pmatrix} 1+\alpha\beta & \beta^2 \\ -\alpha^2 & 1-\alpha\beta \end{pmatrix},$$

where \pm means the equivalence relation $(\alpha \ \beta) \sim (-\alpha \ -\beta)$. We define the operation $*$ on \mathcal{P} by

$$(\alpha \ \beta) * (\gamma \ \delta) := (\alpha \ \beta) \begin{pmatrix} 1+\gamma\delta & \delta^2 \\ -\gamma^2 & 1-\gamma\delta \end{pmatrix} \in (\mathbb{C}^2 \setminus \{0\})/\pm,$$

where the matrix multiplication on the right-hand side is the standard multiplication. (This definition is the transpose of the one used in [Inoue and Kabaya 2014] and [Cho 2016a].) Note that this definition coincides with the operation of the conjugation quandle $(\mathcal{P}, *)$ by

$$\begin{aligned} (\alpha \ \beta) * (\gamma \ \delta) &= (\alpha \ \beta) \begin{pmatrix} 1+\gamma\delta & \delta^2 \\ -\gamma^2 & 1-\gamma\delta \end{pmatrix} \in (\mathbb{C}^2 \setminus \{0\})/\pm \\ &\longleftrightarrow \begin{pmatrix} 1+\gamma\delta & \delta^2 \\ -\gamma^2 & 1-\gamma\delta \end{pmatrix}^{-1} \begin{pmatrix} 1+\alpha\beta & -\alpha^2 \\ \beta^2 & 1-\alpha\beta \end{pmatrix} \begin{pmatrix} 1+\gamma\delta & \delta^2 \\ -\gamma^2 & 1-\gamma\delta \end{pmatrix} \\ &= (\gamma \ \delta)^{-1} (\alpha \ \beta) (\gamma \ \delta) \in \text{PSL}(2, \mathbb{C}). \end{aligned}$$

The inverse operation is given by

$$(\alpha \ \beta) *^{-1} (\gamma \ \delta) = (\alpha \ \beta) \begin{pmatrix} 1-\gamma\delta & -\gamma^2 \\ \delta^2 & 1+\gamma\delta \end{pmatrix}.$$

From now on, we use the notation \mathcal{P} instead of $(\mathbb{C}^2 \setminus \{0\})/\pm$.

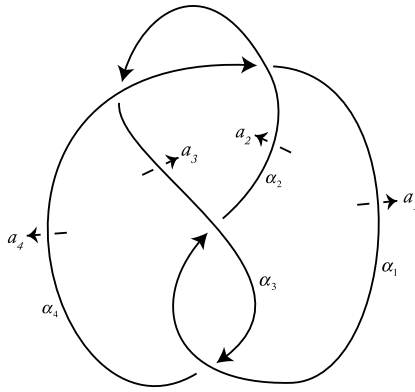


Figure 1. The figure-eight knot 4_1 .

2B. Link group and shadow-coloring. Consider a representation $\rho : \pi_1(L) \rightarrow \text{PSL}(2, \mathbb{C})$ of a hyperbolic link L . We call ρ *boundary-parabolic* when the peripheral subgroup $\pi_1(\partial(\mathbb{S}^3 \setminus L))$ of $\pi_1(L)$ maps to a subgroup of $\text{PSL}(2, \mathbb{C})$ whose elements are all parabolic.

For a fixed oriented link diagram² D of L , Wirtinger presentation gives an algorithmic expression of $\pi_1(L)$. For each arc α_k of D , we draw a small arrow labeled a_k as in Figure 1, which represents a loop. (The details are in [Rolfsen 1976]. Here we are using the opposite orientation of a_k to be consistent with the operation of the conjugation quandle.) This loop corresponds to one of the meridian curves of the boundary tori, so $\rho(a_k)$ is an element in \mathcal{P} . Hence we call $\{\rho(a_1), \dots, \rho(a_n)\}$ the *arc-coloring*³ of D , where each $\rho(a_k)$ is assigned to the corresponding arc α_k .

The Wirtinger presentation of the link group is given by

$$\pi_1(L) = \langle a_1, \dots, a_n ; r_1, \dots, r_n \rangle,$$

where the relation r_l is assigned to each crossing as in Figure 2. Note that r_l coincides with (3), so we can write down the relation of the arc-colors as in Figure 3.

From now on, we always assume $\rho : \pi_1(L) \rightarrow \text{PSL}(2, \mathbb{C})$ is a given boundary-parabolic representation. To avoid redundant notations, arc-coloring will be denoted by $\{a_1, \dots, a_n\}$ without indicating ρ from now on. Choose an element $s_f \in \mathcal{P}$

² We always assume the diagram does not contain a trivial knot component which has only over-crossings or under-crossings or no crossing. (For example, any inseparable link diagram satisfies this condition.) If it happens, then we change the diagram of the trivial component slightly. For example, applying a Reidemeister second move to make different types of crossings or a Reidemeister first move to add a kink is good enough. This assumption is necessary to guarantee that the octahedral triangulation becomes a topological triangulation of $\mathbb{S}^3 \setminus (L \cup \{\text{two points}\})$

³ Strictly speaking, an arc-coloring is a map from arcs of D to \mathcal{P} , not a set. (A region-coloring, which will be defined below, is also a map from regions of D to \mathcal{P} .) However, we abuse the set notation here for convenience.

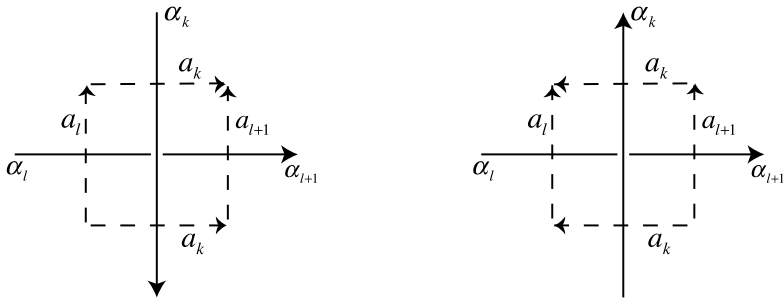


Figure 2. Relations at crossings, where $r_l : a_{l+1} = a_k^{-1} a_l a_k$ (left), or $r_l : a_l = a_k^{-1} a_{l+1} a_k$ (right).

corresponding to a region of the diagram D and determine $s_1, s_2, \dots, s_m \in \mathcal{P}$ corresponding to each regions using the relation in Figure 4.

The assignment of elements of \mathcal{P} to all regions using the relation in Figure 4 is called the *region-coloring*. This assignment is well defined because the two curves in Figure 5, which we call the *cross-changing pair*, determine the same region-coloring, and any pair of curves with the same starting and ending points can be transformed into each other by a finite sequence of cross-changing pairs.

An arc-coloring together with a region-coloring is called a *shadow-coloring*. Lemma 2.4 shows an important property of shadow-colorings, which is crucial for showing the existence of solutions of certain equations.

Definition 2.3. The *Hopf map* $h : \mathcal{P} \longrightarrow \mathbb{C}\mathbb{P}^1 = \mathbb{C} \cup \{\infty\}$ is defined by

$$(\alpha \ \beta) \mapsto \frac{\alpha}{\beta}.$$

Note that $h(\alpha \ \beta) = \alpha/\beta$ is the fixed point of the Möbius transformation

$$f(z) = \frac{(1 + \alpha\beta)z - \alpha^2}{\beta^2 z + (1 - \alpha\beta)}.$$

Lemma 2.4. Let L be a link and assume an arc-coloring is already given by the boundary-parabolic representation $\rho : \pi_1(L) \longrightarrow \text{PSL}(2, \mathbb{C})$. Then there exists a

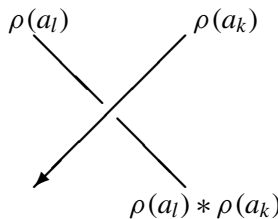


Figure 3. An arc-coloring.

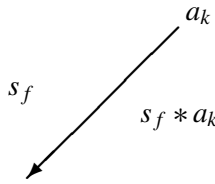


Figure 4. A region-coloring.

region-coloring such that, for any edge of the link diagram with its arc-color a_k ($k = 1, \dots, n$) and its surrounding region-colors $s_f, s_f * a_k$ (see Figure 4), the following holds:

$$(5) \quad h(a_k) \neq h(s_f) \neq h(s_f * a_k) \neq h(a_k).$$

Proof. Note that this was already proved inside the proof of Proposition 2 of [Inoue and Kabaya 2014]. However, finding the proof in the article is not easy, so we write it down below for the readers' convenience.

For the given arc-colors a_1, \dots, a_n , we choose region-colors s_1, \dots, s_m so that

$$(6) \quad \{h(s_1), \dots, h(s_m)\} \cap \{h(a_1), \dots, h(a_n)\} = \emptyset.$$

This is always possible because each $h(s_k)$ is written as $h(s_k) = M_k(h(s_1))$ by a Möbius transformation M_k , which only depends on the arc-colors a_1, \dots, a_r . If we choose $h(s_1) \in \mathbb{C}\mathbb{P}^1$ away from the finite set

$$\bigcup_{1 \leq k \leq n} \{M_k^{-1}(h(a_1)), \dots, M_k^{-1}(h(a_r))\},$$

we have $h(s_k) \notin \{h(a_1), \dots, h(a_r)\}$ for all k . This choice of a region-coloring guarantees $h(a_k) \neq h(s_f)$ and $h(s_f * a_k) \neq h(a_k)$.

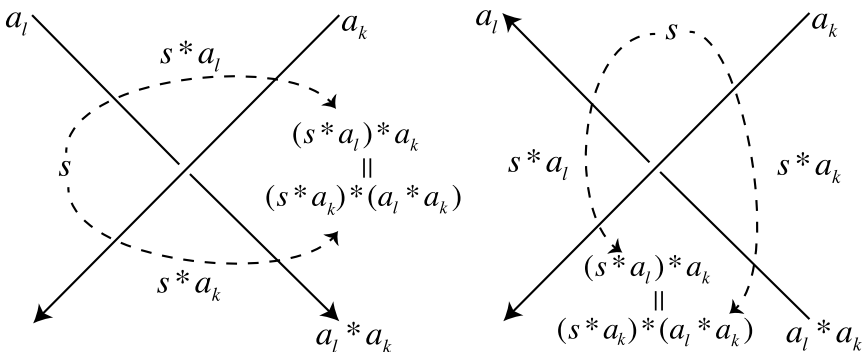


Figure 5. Well-definedness of region-coloring for a positive crossing (left) and a negative crossing (right).

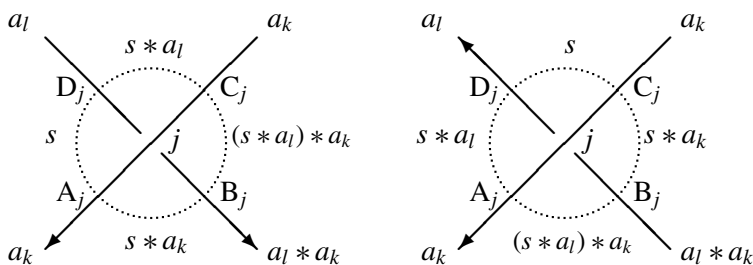


Figure 6. Positive (left) and negative (right) crossings of j with shadow-coloring.

Now assume $h(s_f * a_k) = h(s_f)$ holds under the choice of the region-coloring above. Then we obtain

$$(7) \quad h(s_f * a_k) = \widehat{a}_k(h(s_f)) = h(s_f),$$

where $\widehat{a}_k : \mathbb{C}P^1 \rightarrow \mathbb{C}P^1$ is the Möbius transformation

$$\widehat{a}_k(z) = \frac{(1 + \alpha_k \beta_k)z - \alpha_k^2}{\beta_k^2 z + (1 - \alpha_k \beta_k)}$$

of $a_k = (\alpha_k \ \beta_k)$. Then (7) implies $h(s)$ is the fixed point of \widehat{a}_k , which means $h(a_k) = h(s)$, which contradicts (6). □

We remark that the condition (6) of a region-coloring is stronger than the condition in Lemma 2.4. For example, the region-colorings of the examples in Section 4 satisfy Lemma 2.4, but they do not satisfy (6). Even though we actually proved the stronger condition (6) in the proof, the region-colorings we consider are always assumed to satisfy Lemma 2.4 from now on. The arc-coloring induced by ρ together with the region-coloring satisfying Lemma 2.4 is called the *shadow-coloring induced by ρ* . This shadow-coloring will determine the exact coordinates of points of the octahedral triangulation in the next section.

2C. Octahedral triangulations of link complements. In this section, we describe the ideal triangulation of $S^3 \setminus (L \cup \{\text{two points}\})$ which appeared in [Cho et al. 2014]. Note that this triangulation naturally arises from the link diagram and has been widely used under various names. For example, the software SnapPea used this triangulation to obtain an ideal triangulation of the link complement $S^3 \setminus L$ [Weeks 2005] (see also [Yokota 2011].) Another name of this construction is the *tunnel construction* in [Baseilhac and Benedetti 2007]. It seems the first written appearance of this construction was in [Thurston 1999].

To obtain the triangulation, we consider the crossing j in Figure 6 and place an octahedron $A_j B_j C_j D_j E_j F_j$ on each crossing j as in Figure 7 (left). Then we twist the

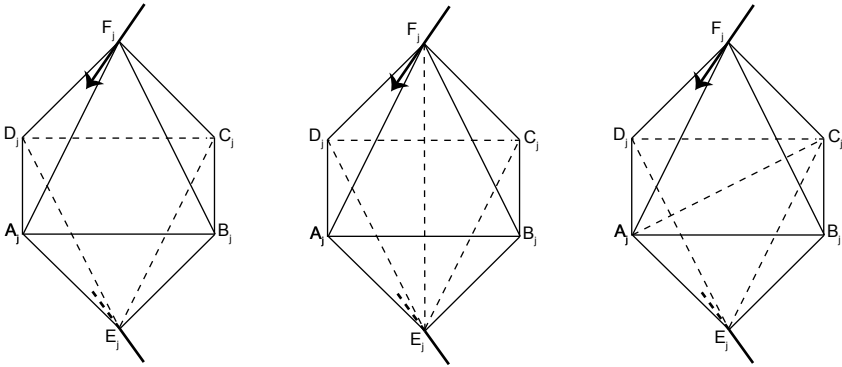


Figure 7. An octahedron on the crossing j .

octahedron by identifying edges $B_j F_j$ to $D_j F_j$ and $A_j E_j$ to $C_j E_j$, respectively. The edges $A_j B_j$, $B_j C_j$, $C_j D_j$ and $D_j A_j$ are called *horizontal edges* and we sometimes express these edges in the diagram as arcs around the crossing as in [Figure 6](#).

Then we glue faces of the octahedra following the lines of the link diagram. Specifically, there are three gluing patterns as in [Figure 8](#). In each of the cases (left, center and right), we identify the faces

$$\begin{aligned} \triangle A_j B_j E_j \cup \triangle C_j B_j E_j & \quad \text{with} \quad \triangle C_{j+1} D_{j+1} F_{j+1} \cup \triangle C_{j+1} B_{j+1} F_{j+1}, \\ \triangle B_j C_j F_j \cup \triangle D_j C_j F_j & \quad \text{with} \quad \triangle D_{j+1} C_{j+1} F_{j+1} \cup \triangle B_{j+1} C_{j+1} F_{j+1}, \\ \triangle A_j B_j E_j \cup \triangle C_j B_j E_j & \quad \text{with} \quad \triangle C_{j+1} B_{j+1} E_{j+1} \cup \triangle A_{j+1} B_{j+1} E_{j+1}, \end{aligned}$$

respectively.

Note that this gluing process identifies vertices $\{A_j, C_j\}$ to one point, denoted by $-\infty$, and $\{B_j, D_j\}$ to another point, denoted by ∞ , and finally $\{E_j, F_j\}$ to the other points, denoted by P_t where $t = 1, \dots, c$ and c is the number of the components of the link L . The regular neighborhoods of $-\infty$ and ∞ are two 3-balls and that of $\bigcup_{t=1}^c P_t$ is a tubular neighborhood of the link L . Therefore, after removing all vertices of the gluing, we obtain an *octahedral decomposition* of $S^3 \setminus (L \cup \{\pm\infty\})$. The *octahedral triangulation* is obtained by subdividing each octahedron of the decomposition into four tetrahedra in a certain way.

To apply the construction of the developing map of ρ in Theorem 4.11 of [[Zickert 2009](#)], we subdivide each octahedron into four tetrahedra using the shadow-coloring of ρ as follows.

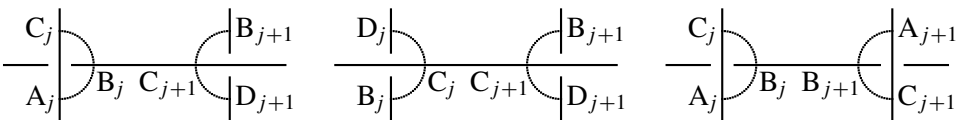


Figure 8. Three gluing patterns.

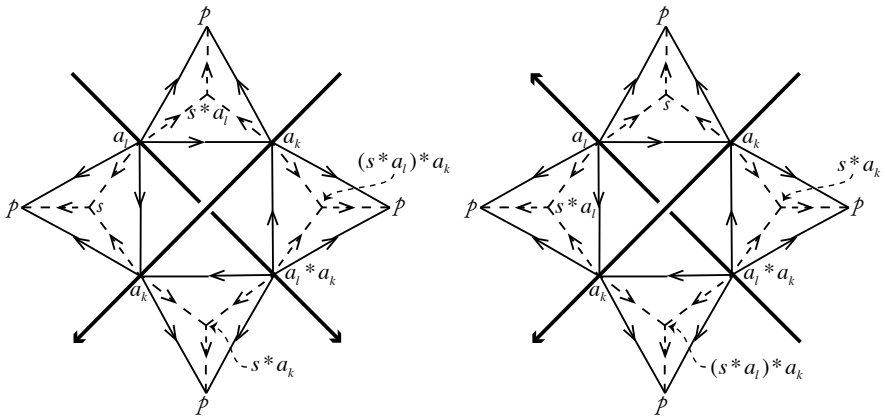


Figure 9. Coordinates of tetrahedra when $h(a_k) \neq h(a_l)$ with a positive crossing (left) and a negative cross (right).

Definition 2.5. Consider a crossing j with the shadow-coloring in Figure 6. The crossing j is called *nondegenerate* when $h(a_k) \neq h(a_l)$ and *degenerate* when $h(a_k) = h(a_l)$.

If a crossing j is nondegenerate, then we subdivide the octahedron on the crossing j into four tetrahedra by adding the edge E_jF_j as in Figure 7 (center). Also, if a crossing j is degenerate, then we subdivide it by adding edge A_jC_j as in Figure 7 (right). This subdivision guarantees nondegeneracy of all tetrahedra, which will be proved at the end of this section. The resulting triangulation is called the *octahedral triangulation* of $\mathbb{S}^3 \setminus (L \cup \{\pm\infty\})$.

Consider the shadow-coloring of a link diagram D induced by ρ , and let $\{a_1, a_2, \dots, a_n\}$ be the arc-colors and $\{s_1, s_2, \dots, s_m\}$ be the region-colors. The number of these colors is finite, so we can choose an element $p \in \mathcal{P}$ satisfying

$$(8) \quad h(p) \notin \{h(a_1), \dots, h(a_n), h(s_1), \dots, h(s_m)\}.$$

The geometric shape of the triangulation is determined by the shadow-coloring induced by ρ in the following way. If the crossing j in Figure 6 is nondegenerate and positive, then let the signed coordinates of the tetrahedra $E_jF_jC_jD_j$, $E_jF_jA_jD_j$, $E_jF_jA_jB_j$, and $E_jF_jC_jB_j$ be

$$(9) \quad \begin{aligned} &(a_l, a_k, s * a_l, p), \\ &-(a_l, a_k, s, p), \\ &(a_l * a_k, a_k, s * a_k, p), \\ &-(a_l * a_k, a_k, (s * a_l) * a_k, p), \end{aligned}$$

respectively. Here, the minus sign of the coordinate means the orientation of the tetrahedron does not coincide with the one induced by the vertex-ordering. Also, if

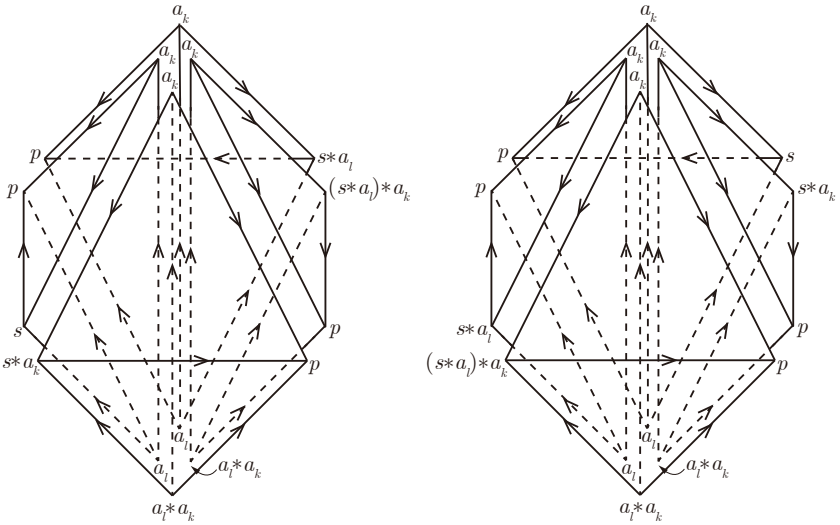


Figure 10. Figure 9 in octahedral position for a positive crossing (left) and a negative crossing (right).

the crossing j is nondegenerate and negative, then let the signed coordinates of the tetrahedra $E_j F_j C_j D_j$, $E_j F_j A_j D_j$, $E_j F_j A_j B_j$, and $E_j F_j C_j B_j$ be

$$\begin{aligned}
 & (a_l, a_k, s, p), \\
 & -(a_l, a_k, s * a_l, p), \\
 (10) \quad & (a_l * a_k, a_k, (s * a_l) * a_k, p), \\
 & -(a_l * a_k, a_k, s * a_k, p),
 \end{aligned}$$

respectively. Figures 9 and 10 show the signed coordinates of (9) and (10).

On the other hand, if the crossing j in Figure 6 is degenerate and is positive, then let the signed coordinates of the tetrahedra $F_j A_j C_j D_j$, $E_j A_j C_j D_j$, $E_j A_j C_j B_j$, and $F_j A_j C_j B_j$ be

$$\begin{aligned}
 & -(a_k, s, s * a_l, p), \\
 & (a_l, s, s * a_l, p), \\
 (11) \quad & -(a_l * a_k, s * a_k, (s * a_l) * a_k, p), \\
 & (a_k, s * a_k, (s * a_l) * a_k, p),
 \end{aligned}$$

respectively. If j is degenerate and negative, then let the signed coordinates be

$$\begin{aligned}
 & -(a_k, s * a_l, s, p), \\
 & (a_l, s * a_l, s, p), \\
 (12) \quad & -(a_l * a_k, (s * a_l) * a_k, s * a_k, p), \\
 & (a_k, (s * a_l) * a_k, s * a_k, p),
 \end{aligned}$$

respectively.

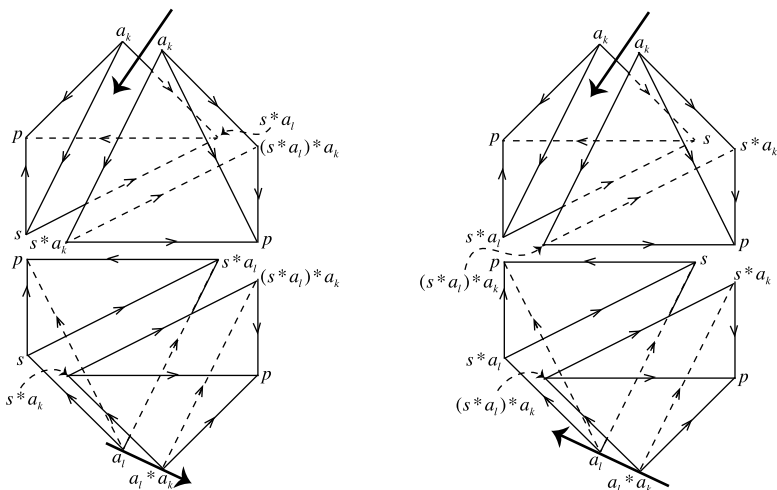


Figure 11. Coordinates of tetrahedra when $h(a_k) = h(a_l)$, for a positive crossing (left) and a negative crossing (right).

Figure 11 shows the signed coordinates of (11) and (12). Note that the orientations of (9)–(12) are different from [Inoue and Kabaya 2014] and match [Cho et al. 2014].

We remark that the signed coordinates (9)–(12) actually define an element in certain simplicial quandle homology in [Inoue and Kabaya 2014]. Although this homology is crucial for proving the main results of [Inoue and Kabaya 2014], we will use their results without the homology.

Definition 2.6. Let $v_0, v_1, v_2, v_3 \in \mathbb{C}\mathbb{P}^1 = \mathbb{C} \cup \{\infty\} = \partial\mathbb{H}^3$. The hyperbolic ideal tetrahedron with signed coordinate $\sigma(v_0, v_1, v_2, v_3)$ with $\sigma \in \{\pm 1\}$ is called *degenerate* when some of the vertices v_0, v_1, v_2, v_3 coincide, and *nondegenerate* when all the vertices are different. The *cross-ratio* $[v_0, v_1, v_2, v_3]^\sigma$ of the nondegenerate signed coordinate $\sigma(v_0, v_1, v_2, v_3)$ is defined by

$$[v_0, v_1, v_2, v_3]^\sigma = \left(\frac{v_3 - v_0}{v_2 - v_0} \frac{v_2 - v_1}{v_3 - v_1} \right)^\sigma \in \mathbb{C} \setminus \{0, 1\}.$$

The tetrahedra in (9)–(12) have elements of the coordinates in \mathcal{P} . Therefore, we need to send them to points in the boundary of the hyperbolic 3-space $\partial\mathbb{H}^3$ so as to obtain hyperbolic ideal tetrahedra. The Hopf map h (see Definition 2.3) plays this role.

Lemma 2.7. *The images of (9)–(12) under the Hopf map h are nondegenerate tetrahedra. Specifically, if the crossing j is nondegenerate and positive, then*

$$\begin{aligned}
 & (h(a_l), h(a_k), h(s * a_l), h(p)), \\
 & -(h(a_l), h(a_k), h(s), h(p)), \\
 & (h(a_l * a_k), h(a_k), h(s * a_k), h(p)), \\
 & -(h(a_l * a_k), h(a_k), h((s * a_l) * a_k), h(p)),
 \end{aligned}
 \tag{13}$$

are nondegenerate hyperbolic ideal tetrahedra and, if the crossing j is nondegenerate and negative, then

$$(14) \quad \begin{aligned} & (h(a_l), h(a_k), h(s), h(p)), \\ & -(h(a_l), h(a_k), h(s * a_l), h(p)), \\ & (h(a_l * a_k), h(a_k), h((s * a_l) * a_k), h(p)), \\ & -(h(a_l * a_k), h(a_k), h(s * a_k), h(p)), \end{aligned}$$

are nondegenerate hyperbolic ideal tetrahedra also.

If the crossing j is degenerate and positive, then

$$(15) \quad \begin{aligned} & (h(a_l), h(s), h(s * a_l), h(p)), \\ & -(h(a_k), h(s), h(s * a_l), h(p)), \\ & (h(a_k), h(s * a_k), h((s * a_l) * a_k), h(p)), \\ & -(h(a_l * a_k), h(s * a_k), h((s * a_l) * a_k), h(p)), \end{aligned}$$

are nondegenerate hyperbolic ideal tetrahedra and, if the crossing j is degenerate and negative, then

$$(16) \quad \begin{aligned} & (h(a_l), h(s * a_l), h(s), h(p)), \\ & -(h(a_k), h(s * a_l), h(s), h(p)), \\ & (h(a_k), h((s * a_l) * a_k), h(s * a_k), h(p)), \\ & -(h(a_l * a_k), h((s * a_l) * a_k), h(s * a_k), h(p)), \end{aligned}$$

are nondegenerate hyperbolic ideal tetrahedra.

Proof. Note that the region-coloring we are considering satisfies [Lemma 2.4](#). To show the nondegeneracy of a tetrahedron, it is enough to show any two endpoints of an edge are different.

In the cases of (13)–(14), endpoints of any edge are adjacent, as a pair among $a_k, s, s * a_k$ in [Figure 4](#) (to check the adjacency, refer to [Figure 5](#)), or one of them is p , except the edges $(a_l, a_k), (a_l * a_k, a_k)$. Therefore, it is enough to show that $h(a_k) \neq h(a_l)$ implies $h(a_l * a_k) \neq h(a_k)$, which is trivial because $h(a_l * a_k) = h(a_k * a_k)$ implies $h(a_l) = h(a_k)$.

In the cases of (15)–(16), all endpoints of edges are adjacent or one of them is p , so we get the proof. \square

Note that, when the crossing j is degenerate, the first two tetrahedra in (15) share the same coordinate with different signs and the others do the same. Therefore, all tetrahedra cancel each other out geometrically and we can remove the octahedron of the crossing. (This is why the crossing is called degenerate.) Also, the same holds for (16). This idea will be used in [Section 3](#).

The assignment of the coordinates to tetrahedra above is from [[Inoue and Kabaya 2014](#)]. Note that this assignment is based on the construction of the developing

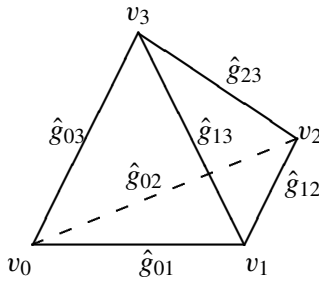


Figure 12. Edge parameters.

map of ρ proposed in [Neumann and Yang 1999] and [Zickert 2009], so the shape of the triangulation determines the developing map of ρ .

2D. Complex volume of ρ . Consider an ideal tetrahedron with vertices $v_0, v_1, v_2,$ and v_3 , where $v_k \in \mathbb{C}\mathbb{P}^1$. For each edge v_kv_l , we assign g_{kl} and $\hat{g}_{kl} \in \mathbb{C}\mathbb{P}^1$, and call them *long-edge parameter* and *edge parameter*, respectively. (See Figure 12.) Later, we will distinguish them by considering that g_{kl} is assigned to the edge of a triangulation and \hat{g}_{kl} to the edge of a tetrahedron.

Definition 2.8. For the edge parameter \hat{g}_{kl} of an ideal tetrahedron, the *Ptolemy relation* is the following equation:

$$\hat{g}_{02}\hat{g}_{13} = \hat{g}_{01}\hat{g}_{23} + \hat{g}_{03}\hat{g}_{12}.$$

For example, if we define the edge parameter $\hat{g}_{kl} := v_l - v_k$, then direct calculation shows

$$(17) \quad (v_2 - v_0)(v_3 - v_1) = (v_1 - v_0)(v_3 - v_2) + (v_3 - v_0)(v_2 - v_1),$$

which is the Ptolemy relation. Furthermore, these edge parameters satisfy

$$(18) \quad [v_0, v_1, v_2, v_3] = \frac{\hat{g}_{03}\hat{g}_{12}}{\hat{g}_{02}\hat{g}_{13}}.$$

To apply the results of [Zickert 2009] and [Hikami and Inoue 2015], the edge parameters should satisfy the Ptolemy relation, (18) and one more condition that they should depend on the edge of the triangulation, not of the tetrahedron. In other words, if two edges are glued in the triangulation, the edge parameters should be the same. We call this latter condition the *coincidence condition*. When the edge-parameters satisfy the coincidence condition, we call them the *long-edge parameters* and denote this by g_{kl} . (We also need the extra condition that the orientations of the two glued edges induced by the vertex-orientations of each tetrahedron should coincide. However, the vertex-orientation in (13)–(16) always satisfies this.) Unfortunately, the edge-parameter $\hat{g}_{kl} = v_l - v_k$ defined above does not satisfy this condition, so we will redefine the edge-parameter and the long-edge parameter using [Inoue and Kabaya 2014] as follows.

At first, consider two elements $a = (\alpha_1 \ \alpha_2)$, $b = (\beta_1 \ \beta_2)$ in \mathcal{P} . We define the *determinant* $\det(a, b)$ by

$$\det(a, b) := \pm \det \begin{pmatrix} \alpha_1 & \alpha_2 \\ \beta_1 & \beta_2 \end{pmatrix} = \pm(\alpha_1\beta_2 - \alpha_2\beta_1).$$

Note that the determinant is defined up to sign due to the choice of the representative $a = (\alpha_1 \ \alpha_2) = (-\alpha_1 \ -\alpha_2) \in \mathcal{P}$. To remove this ambiguity, we fix representatives⁴ of arc-colors in $\mathbb{C}^2 \setminus \{0\}$ once and for all. Then we fix a representative of one region-color, which uniquely determines the representatives of all the other region-colors by the arc-coloring. (This is due to the fact that $s * (\pm a) = s * a$ for any $s, a \in \mathbb{C}^2 \setminus \{0\}$.)

After fixing all the representatives of the shadow-coloring, we obtain a well-defined determinant

$$(19) \quad \det(a, b) = \det \begin{pmatrix} \alpha_1 & \alpha_2 \\ \beta_1 & \beta_2 \end{pmatrix} = \alpha_1\beta_2 - \alpha_2\beta_1.$$

Lemma 2.9. *For $a, b, c \in \mathbb{C}^2 \setminus \{0\}$, the determinant satisfies*

$$\det(a * c, b * c) = \det(a, b).$$

Proof. Let $a = (\alpha_1 \ \alpha_2)$, $b = (\beta_1 \ \beta_2)$, $c = (\gamma_1 \ \gamma_2)$, and

$$C = \begin{pmatrix} 1 + \gamma_1\gamma_2 & \gamma_2^2 \\ -\gamma_1^2 & 1 - \gamma_1\gamma_2 \end{pmatrix}.$$

Then

$$\det(a * c, b * c) = \det(aC, bC) = \det(a, b) \cdot \det C = \det(a, b). \quad \square$$

Consider the shadow-coloring and the coordinates of tetrahedra in [Figure 9](#) (or [Figure 10](#)) and [Figure 11](#). We define the edge parameter \hat{g}_{kl} using those coordinates. Specifically, when the signed coordinate of the tetrahedron is $\sigma(a_0, a_1, a_2, a_3)$ with $\sigma \in \{\pm 1\}$ and $a_k \in \mathbb{C}^2 \setminus \{0\}$, we define the edge parameter by

$$(20) \quad \hat{g}_{kl} = \det(a_k, a_l).$$

For example, the edge parameters of the tetrahedron $\mp(a_l, a_k, s, p)$ in the left-hand or the right-hand side of [Figure 9](#) (or [Figure 10](#)) are defined by

$$\begin{aligned} \hat{g}_{01} &= \det(a_l, a_k), & \hat{g}_{02} &= \det(a_l, s), & \hat{g}_{03} &= \det(a_l, p), \\ \hat{g}_{12} &= \det(a_k, s), & \hat{g}_{13} &= \det(a_k, p), & \hat{g}_{23} &= \det(s, p). \end{aligned}$$

⁴ The difference in [\[Inoue and Kabaya 2014\]](#) is that they chose a sign of the determinant once and for all. Their choice is good enough to define the long-edge parameter g_{jk} , but not for the edge parameter \hat{g}_{jk} .

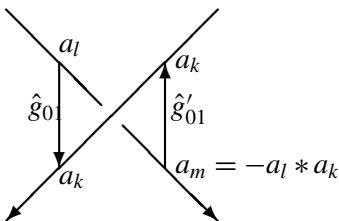


Figure 13. An example of the inconsistency of the edge parameter.

Lemma 2.10. *The edge parameter \hat{g}_{kl} of the tetrahedron $\sigma(a_0, a_1, a_2, a_3)$ defined in (20) satisfies the Ptolemy identity and*

$$(21) \quad [h(a_0), h(a_1), h(a_2), h(a_3)] = \frac{\hat{g}_{03}\hat{g}_{12}}{\hat{g}_{02}\hat{g}_{13}}.$$

Proof. From (19), we obtain

$$(22) \quad h(x) - h(y) = \frac{x_1}{x_2} - \frac{y_1}{y_2} = \frac{\det(x, y)}{x_2 y_2},$$

where $x = (x_1 \ x_2)$ and $y = (y_1 \ y_2)$.

Let $a_k = (\alpha_k \ \beta_k)$ for $k = 0, \dots, 3$, and let $v_k = h(a_k) = \alpha_k / \beta_k$. Then (17) and (22) imply

$$\frac{\det(a_0, a_2)}{\beta_0 \beta_2} \frac{\det(a_1, a_3)}{\beta_1 \beta_3} = \frac{\det(a_0, a_1)}{\beta_0 \beta_1} \frac{\det(a_2, a_3)}{\beta_2 \beta_3} + \frac{\det(a_0, a_3)}{\beta_0 \beta_3} \frac{\det(a_1, a_2)}{\beta_1 \beta_2},$$

which is equivalent to the Ptolemy identity $\hat{g}_{02}\hat{g}_{13} = \hat{g}_{01}\hat{g}_{23} + \hat{g}_{03}\hat{g}_{12}$.

Also, using (22), we obtain

$$[h(a_0), h(a_1), h(a_2), h(a_3)] = \frac{\frac{\det(a_0, a_3)}{\beta_0 \beta_3} \frac{\det(a_1, a_2)}{\beta_1 \beta_2}}{\frac{\det(a_1, a_3)}{\beta_1 \beta_3} \frac{\det(a_0, a_2)}{\beta_0 \beta_2}} = \frac{\hat{g}_{03}\hat{g}_{12}}{\hat{g}_{02}\hat{g}_{13}}. \quad \square$$

Note that, by the same calculation as in the proof above, we obtain

$$[h(a_0), h(a_3), h(a_1), h(a_2)] = \frac{\hat{g}_{02}\hat{g}_{13}}{\hat{g}_{01}\hat{g}_{23}}, \quad [h(a_0), h(a_2), h(a_3), h(a_1)] = -\frac{\hat{g}_{01}\hat{g}_{23}}{\hat{g}_{03}\hat{g}_{12}}.$$

If we put $z^\sigma = [h(a_0), h(a_1), h(a_2), h(a_3)]$, using the Ptolemy identity, the above equations are expressed by

$$(23) \quad z^\sigma = \frac{\hat{g}_{03}\hat{g}_{12}}{\hat{g}_{02}\hat{g}_{13}}, \quad \frac{1}{1 - z^\sigma} = \frac{\hat{g}_{02}\hat{g}_{13}}{\hat{g}_{01}\hat{g}_{23}}, \quad 1 - \frac{1}{z^\sigma} = -\frac{\hat{g}_{01}\hat{g}_{23}}{\hat{g}_{03}\hat{g}_{12}}.$$

The edge parameter \hat{g}_{jk} defined above satisfies all needed properties of the long-edge parameter g_{jk} except the *coincidence*, which \hat{g}_{jk} satisfies up to sign. To see this phenomenon, consider the two edges of Figure 9 (left) as in Figure 13,

which are glued in the triangulation. Assume the chosen representative of a_m in [Figure 13](#) satisfies $a_m = -a_l * a_k \in \mathbb{C}^2 \setminus \{0\}$. (This actually happens often and is quite important. For example, the minus signs of [\(49\)](#) and [\(50\)](#) in [Section 4](#) show this situation. This scenario will be discussed in depth in a later article.) Then the edge parameters satisfy

$$\hat{g}_{01} = \det(a_l, a_k) = \det(a_l * a_k, a_k) = -\det(a_m, a_k) = -\hat{g}'_{01}.$$

To obtain the long-edge parameter g_{jk} , we assign certain signs to the edge parameters

$$g_{jk} = \pm \hat{g}_{jk},$$

so that the consistency property holds. Due to [Lemma 6](#) of [\[Inoue and Kabaya 2014\]](#), any choice of values of g_{jk} determines the same complex volume. Actually, in [Section 3](#), we do not need the exact values of g_{jk} , but we use the existence of them.

The relations of the edge parameters in [\(23\)](#) become

$$(24) \quad z^\sigma = \pm \frac{g_{03}g_{12}}{g_{02}g_{13}}, \quad \frac{1}{1-z^\sigma} = \pm \frac{g_{02}g_{13}}{g_{01}g_{23}}, \quad 1 - \frac{1}{z^\sigma} = \pm \frac{g_{01}g_{23}}{g_{03}g_{12}}.$$

Using [\(24\)](#), we define integers p and q by

$$(25) \quad \begin{cases} p\pi i = -\log z^\sigma + \log g_{03} + \log g_{12} - \log g_{02} - \log g_{13}, \\ q\pi i = \log(1 - z^\sigma) + \log g_{02} + \log g_{13} - \log g_{01} - \log g_{23}. \end{cases}$$

Now we consider the tetrahedron with the signed coordinate $\sigma(a_0, a_1, a_2, a_3)$ and the signed triples $\sigma[z^\sigma; p, q] \in \widehat{\mathcal{P}}(\mathbb{C})$. (The *extended pre-Bloch group* is denoted by $\widehat{\mathcal{P}}(\mathbb{C})$ here. For the definition, see [Definition 1.6](#) of [\[Zickert 2009\]](#).) To consider all signed triples corresponding to all tetrahedra in the triangulation, we denote the triple by $\sigma_t[z_t^{\sigma_t}; p_t, q_t]$, where t is the index of tetrahedra. We define a function $\widehat{L} : \widehat{\mathcal{P}}(\mathbb{C}) \rightarrow \mathbb{C}/\pi^2\mathbb{Z}$ by

$$(26) \quad [z; p, q] \mapsto \text{Li}_2(z) + \frac{1}{2} \log z \log(1 - z) + \frac{\pi i}{2} (q \log z + p \log(1 - z)) - \frac{\pi^2}{6},$$

where $\text{Li}_2(z) = -\int_0^z \frac{1}{t} \log(1 - t) dt$ is the dilogarithm function. (Well-definedness of \widehat{L} was proved in [\[Neumann 2004\]](#).) Recall that, for a boundary-parabolic representation ρ , the hyperbolic volume $\text{vol}(\rho)$ and the Chern–Simons invariant $\text{cs}(\rho)$ were already defined in [\[Zickert 2009\]](#). We call $\text{vol}(\rho) + i \text{cs}(\rho)$ the *complex volume of ρ* . The following theorem is one of the main results of [\[Inoue and Kabaya 2014\]](#).

Theorem 2.11 [\[Zickert 2009; Inoue and Kabaya 2014\]](#). *For a given boundary-parabolic representation ρ and the shadow-coloring induced by ρ , the complex*

volume of ρ is calculated by

$$\sum_t \sigma_t \widehat{L}[z_t^{\sigma_t}; p_t, q_t] \equiv i(\text{vol}(\rho) + i \text{cs}(\rho)) \pmod{\pi^2},$$

where t is over all tetrahedra of the triangulation defined in Section 2C.

Proof. See Theorem 5 of [Inoue and Kabaya 2014]. □

Note that the removal of the tetrahedra in (15) and (16) does not have any effect on the complex volume. For example, if we let $[z; p, q]$ and $-[z'; p', q']$ be the corresponding triples of the tetrahedron $(h(a_l), h(s), h(s * a_l), h(p))$ and $-(h(a_k), h(s), h(s * a_l), h(p))$ in (15), respectively, and put $\{g_{kl}\}, \{g'_{kl}\}$ the sets of long-edge parameters of the two tetrahedra, respectively, then, from $h(a_l) = h(a_k)$, we obtain $z = z'$. Furthermore, we can choose long-edge parameters so that $g_{kl} = g'_{kl}$ holds for all pairs of edges sharing the same coordinate, which induces $p = p', q = q'$ and $\widehat{L}[z; p, q] - \widehat{L}[z'; p', q'] = 0$.

3. Optimistic limit

In this section, we will use the result of Section 2 to redefine the optimistic limit of [Cho et al. 2014] and construct a solution of \mathcal{H} . At first, we consider a given boundary-parabolic representation ρ and fix its shadow-coloring of a link diagram D . For the diagram, define the sides of the diagram to be the lines connecting two adjacent crossings. (The word *edge* is more common than *side* here. However, we want to keep the word *edge* for the edges of a triangulation.) For example, the diagram in Figure 14 has eight sides. We assign z_1, \dots, z_n to sides of D as in Figure 14 and call them *side variables*.

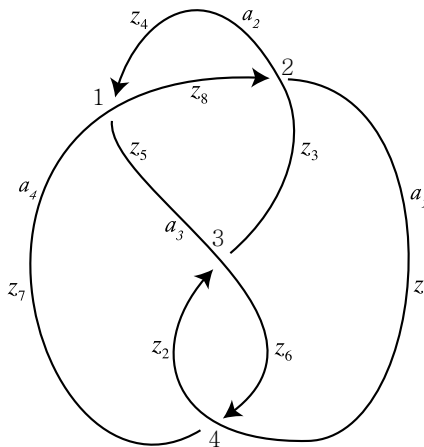


Figure 14. Sides of a link diagram.

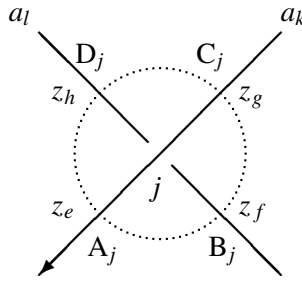


Figure 15. A crossing j with arc-colors and side variables.

For the crossing j in Figure 15, let z_e, z_f, z_g, z_h be side variables and let a_l, a_k be the arc-colors. If $h(a_k) \neq h(a_l)$, then we define the potential function V_j of the crossing j by

$$(27) \quad V_j(z_e, z_f, z_g, z_h) = \text{Li}_2\left(\frac{z_f}{z_e}\right) - \text{Li}_2\left(\frac{z_f}{z_g}\right) + \text{Li}_2\left(\frac{z_h}{z_g}\right) - \text{Li}_2\left(\frac{z_h}{z_e}\right).$$

On the other hand, if $h(a_l) = h(a_k)$ in Figure 15, then we introduce new variables w_e^j, w_f^j, w_g^j of the crossing j and define

$$(28) \quad V_j(z_e, z_f, z_g, z_h, w_e^j, w_f^j, w_g^j) \\ = -\log w_e^j \log z_e + \log w_f^j \log z_f - \log w_g^j \log z_g + \log(w_e^j w_g^j / w_f^j) \log z_h.$$

For notational convenience, we put $w_h^j := w_e^j w_g^j / w_f^j$. (In (28), we can choose any three variables among $w_e^j, w_f^j, w_g^j, w_h^j$ free variables.) We call the crossing j in Figure 15 *degenerate* when $h(a_l) = h(a_k)$ holds. In particular, when the degenerate crossing forms a kink, as in Figure 16, we put

$$V_j(z_e, z_f, z_g, w_e^j, w_f^j) \\ = -\log w_e^j \log z_e + \log w_f^j \log z_f - \log w_f^j \log z_f + \log(w_e^j w_f^j / w_f^j) \log z_g \\ = -\log w_e^j \log z_e + \log w_f^j \log z_g.$$

Consider the crossing j in Figure 15 and place the octahedron $A_j B_j C_j D_j E_j F_j$ as in Figure 7. When the crossing j is nondegenerate, in other words $h(a_k) \neq h(a_l)$, we consider Figure 7 (center) and assign shape parameters $z_f/z_e, z_g/z_f, z_h/z_g$ and z_e/z_h to the horizontal edges $A_j B_j, B_j C_j, C_j D_j, D_j A_j$, respectively. On the other hand, if the crossing j is degenerate, in other words $h(a_k) = h(a_l)$, then we

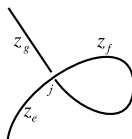


Figure 16. A kink.

consider [Figure 7](#) (right) and assign shape parameters w_e^j, w_f^j, w_g^j and w_h^j to the edges A_jF_j, B_jE_j, C_jF_j and D_jE_j , respectively.⁵

The potential function $V(z_1, \dots, z_n, w_k^j, \dots)$ of the link diagram D is defined by

$$V(z_1, \dots, z_n, w_k^j, \dots) = \sum V_j,$$

where j is over all crossings. For example, if $h(a_1^j) \neq h(a_2)$ in [Figure 14](#), then $a_4 = a_1 * a_2$ implies⁶ $h(a_4) \neq h(a_2)$, $a_2 = a_1 * a_3$ implies⁷ $h(a_2) \neq h(a_3) \neq h(a_1)$, $a_2 = a_3 * a_4$ implies $h(a_4) \neq h(a_3)$, $a_4 = a_3 * a_1$ implies $h(a_4) \neq h(a_1)$, and the potential function becomes

$$(29) \quad V(z_1, \dots, z_8) = \left\{ \text{Li}_2\left(\frac{z_5}{z_7}\right) - \text{Li}_2\left(\frac{z_5}{z_8}\right) + \text{Li}_2\left(\frac{z_4}{z_8}\right) - \text{Li}_2\left(\frac{z_4}{z_7}\right) \right\} \\ + \left\{ \text{Li}_2\left(\frac{z_1}{z_3}\right) - \text{Li}_2\left(\frac{z_1}{z_4}\right) + \text{Li}_2\left(\frac{z_8}{z_4}\right) - \text{Li}_2\left(\frac{z_8}{z_3}\right) \right\} \\ + \left\{ \text{Li}_2\left(\frac{z_3}{z_6}\right) - \text{Li}_2\left(\frac{z_3}{z_5}\right) + \text{Li}_2\left(\frac{z_2}{z_5}\right) - \text{Li}_2\left(\frac{z_2}{z_6}\right) \right\} \\ + \left\{ \text{Li}_2\left(\frac{z_6}{z_1}\right) - \text{Li}_2\left(\frac{z_6}{z_2}\right) + \text{Li}_2\left(\frac{z_7}{z_2}\right) - \text{Li}_2\left(\frac{z_7}{z_1}\right) \right\}.$$

Note that, if $h(a_l) \neq h(a_k)$ for any crossing j in [Figure 15](#), then the definition of the potential function above coincides with the definition in Section 2 of [[Cho et al. 2014](#)]. Therefore, the above definition is a slight modification of the previous one.

On the other hand, if $h(a_1) = h(a_2)$ in [Figure 14](#), then $a_1 * a_2 = a_1$. This equation and the relations at crossings induce⁸ $a_1 = a_2 = a_3 = a_4$, and the potential function becomes

$$V(z_1, \dots, z_8, w_8^1, w_4^1, w_7^1, w_4^2, w_8^2, w_3^2, w_6^2, w_3^3, w_3^3, w_5^3, w_2^4, w_7^4, w_1^4) = \\ - \log w_8^1 \log z_8 + \log w_4^1 \log z_4 - \log w_7^1 \log z_7 + \log w_5^1 \log z_5 \\ - \log w_4^2 \log z_4 + \log w_8^2 \log z_8 - \log w_3^2 \log z_3 + \log w_1^2 \log z_1 \\ - \log w_6^3 \log z_6 + \log w_3^3 \log z_3 - \log w_5^3 \log z_5 + \log w_2^3 \log z_2 \\ - \log w_2^4 \log z_2 + \log w_7^4 \log z_7 - \log w_1^4 \log z_1 + \log w_6^4 \log z_6,$$

⁵ Note that, when $h(a_k) = h(a_l)$, by adding one more edge B_jD_j to [Figure 7](#) (right), we obtain another subdivision of the octahedron with five tetrahedra. (This subdivision was already used in [[Cho 2016b](#)].) Focusing on the middle tetrahedron that contains all horizontal edges, we obtain $w_e^j w_g^j = w_f^j w_h^j$. Furthermore, the shape-parameters assigned to D_jF_j and B_jF_j are $(1 - 1/w_e^j)/(1 - w_g^j)$ and $(1 - 1/w_g^j)/(1 - w_e^j)$, respectively.

⁶ If $h(a_4) = h(a_2)$, then $h(a_2 * a_2) = h(a_2) = h(a_4) = h(a_1 * a_2)$ induces $h(a_2) = h(a_1)$, which is a contradiction.

⁷ If $h(a_2) = h(a_3)$, then $h(a_3 * a_3) = h(a_3) = h(a_2) = h(a_1 * a_3)$ induces $h(a_2) = h(a_3) = h(a_1)$, which is a contradiction. Likewise, if $h(a_1) = h(a_3)$, then $h(a_2) = h(a_1 * a_3) = h(a_1)$ is a contradiction.

⁸ The relation $a_4 = a_1 * a_2$ induces $a_4 = a_1$, $a_4 = a_3 * a_1$ induces $a_4 = a_3$, and $a_2 = a_3 * a_4$ induces $a_2 = a_4$.

where $w_5^1 = w_8^1 w_7^1 / w_4^1$, $w_1^2 = w_4^2 w_3^2 / w_8^2$, $w_2^3 = w_6^3 w_5^3 / w_3^3$ and $w_6^4 = w_2^4 w_1^4 / w_7^4$.

For the potential function $V(z_1, \dots, z_n, w_k^j, \dots)$, let \mathcal{H} be the set of equations

$$(30) \quad \mathcal{H} := \left\{ \exp\left(z_k \frac{\partial V}{\partial z_k}\right) = 1, \exp\left(w_k^j \frac{\partial V}{\partial w_k^j}\right) = 1 \mid k = 1, \dots, n, j : \text{degenerate} \right\},$$

and $\mathcal{S} = \{(z_1, \dots, z_n, w_k^j, \dots)\}$ be the solution set of \mathcal{H} . Here, solutions are assumed to satisfy the properties that $z_k \neq 0$ for all $k = 1, \dots, n$ and $z_f/z_e \neq 1$, $z_g/z_f \neq 1$, $z_h/z_g \neq 1$, $z_e/z_h \neq 1$, $z_g/z_e \neq 1$, $z_h/z_f \neq 1$ in Figure 15 for any nondegenerate crossing, and $w_k^j \neq 0$ for any degenerate crossing j and the index k . (All these assumptions are essential to avoid singularity of the equations in \mathcal{H} and $\log 0$ in the formula V_0 defined in (1). Even though we allow $w_k^j = 1$ here, the value we are interested in always satisfies $w_k^j \neq 1$.)

Proposition 3.1. *For the arc-coloring of a link diagram D induced by ρ and the potential function $V(z_1, \dots, z_n, w_k^j, \dots)$, the set \mathcal{H} induces the whole set of hyperbolicity equations of the octahedral triangulation defined in Section 2C.*

The hyperbolicity equations consist of Thurston’s gluing equations of edges and the completeness condition.

Proof of Proposition 3.1. For the case where no crossing is degenerate, this proposition was already proved in Section 3 of [Cho et al. 2014]. To see the main idea, check Figures 10–13 and equations (3.1)–(3.3) of [Cho et al. 2014]. Equation (3.1) is a completeness condition along a meridian of a certain annulus, and (3.2)–(3.3) are gluing equations of certain edges. These three types of equations induce all the other gluing equations.

Therefore, we consider the case when the crossing j in Figure 15 is degenerate. Then, the three equations

$$(31) \quad \exp\left(w_e^j \frac{\partial V}{\partial w_e^j}\right) = \frac{z_h}{z_e} = 1, \exp\left(w_f^j \frac{\partial V}{\partial w_f^j}\right) = \frac{z_f}{z_h} = 1, \exp\left(w_g^j \frac{\partial V}{\partial w_g^j}\right) = \frac{z_h}{z_g} = 1$$

induce $z_e = z_f = z_g = z_h$. This guarantees the gluing equations of horizontal edges trivially by the assigning rule of shape parameters. (Note that the shape parameters assigned to the horizontal edges of the octahedron at a degenerate crossing are always 1.)

There are four possible cases of gluing pattern as in Figure 17, and we assume the crossing j is degenerate and $j + 1$ is nondegenerate. (The case when both of j and $j + 1$ are degenerate can be proved similarly.)

The part of the potential function V containing z_k in Figure 17 (top left) is

$$V^{(a)} = \log w_k^j \log z_k + \text{Li}_2\left(\frac{z_e}{z_k}\right) - \text{Li}_2\left(\frac{z_f}{z_k}\right),$$

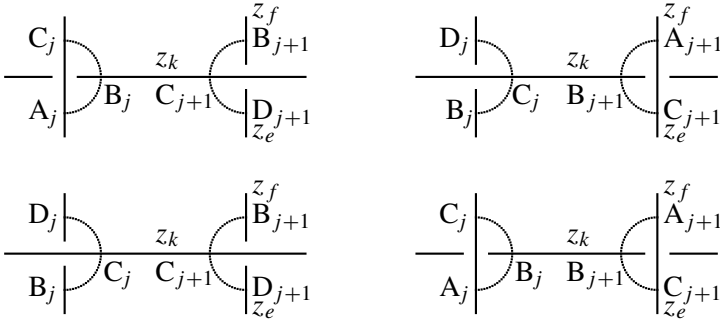


Figure 17. Four cases of a gluing pattern.

and

$$\exp\left(z_k \frac{\partial V}{\partial z_k}\right) = \exp\left(z_k \frac{\partial V^{(a)}}{\partial z_k}\right) = w_k^j \left(1 - \frac{z_e}{z_k}\right) \left(1 - \frac{z_f}{z_k}\right)^{-1} = 1$$

is equivalent to the following completeness condition

$$\frac{1}{w_k^j} \left(1 - \frac{z_e}{z_k}\right)^{-1} \left(1 - \frac{z_f}{z_k}\right) = 1$$

along a meridian m in [Figure 18](#) (top left). (Compare it with [Figure 11](#) of [\[Cho et al. 2014\]](#).) Here, $a_j, b_j, c_j, b_{j+1}, c_{j+1}, d_{j+1}$ in [Figure 18](#) (top left) are the points of the cusp diagram, which lie on the edges $A_jE_j, B_jE_j, C_jE_j, B_{j+1}F_{j+1}, C_{j+1}F_{j+1}, D_{j+1}F_{j+1}$ of [Figure 7](#) (left), respectively.

The part of the potential function V containing z_k in [Figure 17](#) (top right) is

$$V^{(b)} = -\log w_k^j \log z_k - \text{Li}_2\left(\frac{z_k}{z_e}\right) + \text{Li}_2\left(\frac{z_k}{z_f}\right),$$

and

$$\exp\left(z_k \frac{\partial V}{\partial z_k}\right) = \exp\left(z_k \frac{\partial V^{(b)}}{\partial z_k}\right) = \frac{1}{w_k^j} \left(1 - \frac{z_k}{z_e}\right) \left(1 - \frac{z_k}{z_f}\right)^{-1} = 1$$

is equivalent to the completeness condition

$$\frac{1}{w_k^j} \left(1 - \frac{z_k}{z_f}\right)^{-1} \left(1 - \frac{z_k}{z_e}\right) = 1$$

along a meridian m in [Figure 18](#) (top right). Here, $b_j, c_j, d_j, a_{j+1}, b_{j+1}, c_{j+1}$ in [Figure 18](#) (top right) are the points of the cusp diagram, which lie on the edges $B_jF_j, C_jF_j, D_jF_j, A_{j+1}E_{j+1}, B_{j+1}E_{j+1}, C_{j+1}E_{j+1}$ of [Figure 7](#) (left), respectively. (To simplify the cusp diagram in [Figure 18](#) (top right), we subdivided the polygon $A_jB_jC_jD_jF_j$ in [Figure 7](#) (right) into three tetrahedra by adding the edge B_jD_j .)

The part of the potential function V containing z_k in [Figure 17](#) (bottom left) is

$$V^{(c)} = -\log w_k^j \log z_k + \text{Li}_2\left(\frac{z_e}{z_k}\right) - \text{Li}_2\left(\frac{z_f}{z_k}\right),$$

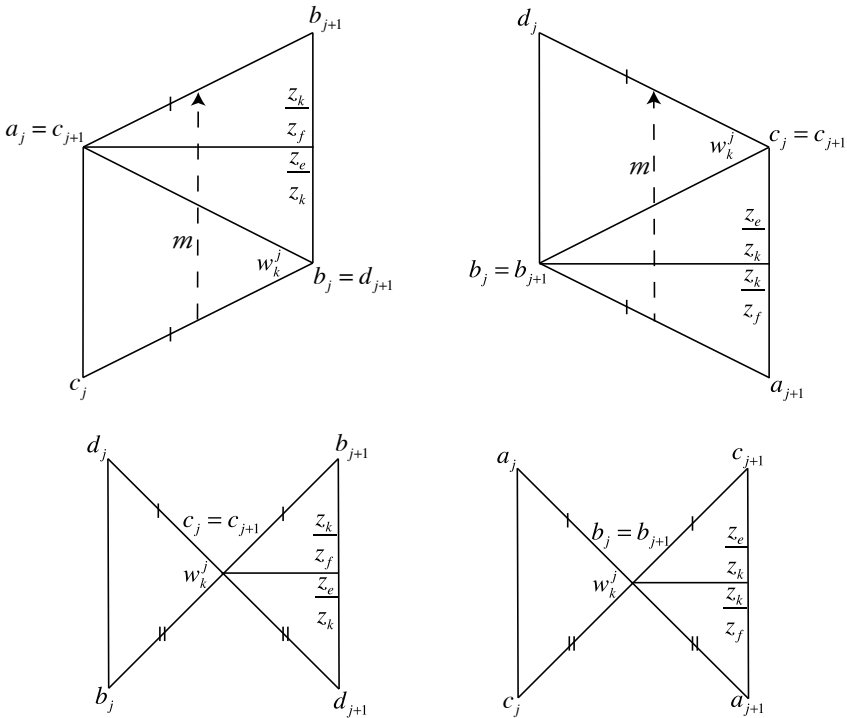


Figure 18. Four cusp diagrams from Figure 17.

and

$$\exp\left(z_k \frac{\partial V}{\partial z_k}\right) = \exp\left(z_k \frac{\partial V^{(c)}}{\partial z_k}\right) = \frac{1}{w_k^j} \left(1 - \frac{z_e}{z_k}\right) \left(1 - \frac{z_f}{z_k}\right)^{-1} = 1$$

is equivalent to the gluing equation

$$w_k^j \left(1 - \frac{z_e}{z_k}\right)^{-1} \left(1 - \frac{z_f}{z_k}\right) = 1$$

of $c_j = c_{j+1}$ in Figure 18 (bottom left). (Compare it with Figure 12 of [Cho et al. 2014].) Here, $b_j, c_j, d_j, b_{j+1}, c_{j+1}, d_{j+1}$ in Figure 18 (bottom left) are the points of the cusp diagram, which lie on the edges $B_jF_j, C_jF_j, D_jF_j, B_{j+1}F_{j+1}, C_{j+1}F_{j+1}, D_{j+1}F_{j+1}$ of Figure 7 (left), respectively, and the edges d_jc_j and b_jc_j are identified to $b_{j+1}c_{j+1}$ and $d_{j+1}c_{j+1}$, respectively. (To simplify the cusp diagram in Figure 18 (bottom left), we subdivided the polygon $A_jB_jC_jD_jF_j$ in Figure 7 (right) into three tetrahedra by adding the edge B_jD_j .)

The part of the potential function V containing z_k in Figure 17 (bottom right) is

$$V^{(d)} = \log w_k^j \log z_k - \text{Li}_2\left(\frac{z_k}{z_e}\right) + \text{Li}_2\left(\frac{z_k}{z_f}\right),$$

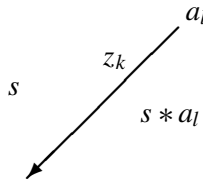


Figure 19. A region-coloring.

and

$$\exp\left(z_k \frac{\partial V}{\partial z_k}\right) = \exp\left(z_k \frac{\partial V^{(d)}}{\partial z_k}\right) = w_k^j \left(1 - \frac{z_k}{z_e}\right) \left(1 - \frac{z_k}{z_f}\right)^{-1} = 1$$

is equivalent to the gluing equation

$$w_k^j \left(1 - \frac{z_k}{z_e}\right) \left(1 - \frac{z_k}{z_f}\right)^{-1} = 1$$

of $b_j = b_{j+1}$ in Figure 18 (bottom right). (Compare it with Figure 13 of [Cho et al. 2014].) Here, $a_j, b_j, c_j, a_{j+1}, b_{j+1}, c_{j+1}$ in Figure 18 (bottom right) are the points of the cusp diagram, which lie on the edges $A_jE_j, B_jE_j, C_jE_j, A_{j+1}E_{j+1}, B_{j+1}E_{j+1}, C_{j+1}E_{j+1}$ of Figure 7 (left), respectively, and the edges a_jb_j and c_jb_j are identified to $c_{j+1}b_{j+1}$ and $a_{j+1}b_{j+1}$, respectively.

Note that the case when both of the crossings j and $j + 1$ in Figure 17 are degenerate can be proved in the same way.

On the other hand, it was already shown in [Cho et al. 2014] that all hyperbolicity equations are induced by these types of equations (see the discussion that follows Lemma 3.1 of [Cho et al. 2014]), so the proof is done. \square

In [Cho et al. 2014], we could not prove the existence of a solution of \mathcal{H} , in other words $\mathcal{S} \neq \emptyset$, so we assumed it. However, the following theorem proves the existence by directly constructing one solution from the given boundary-parabolic representation ρ together with the shadow-coloring.

Theorem 3.2. Consider a shadow-coloring of a link diagram D induced by ρ and the potential function $V(z_1, \dots, z_n, w_k^j, \dots)$ from D . For each side of D with the side variable z_k , arc-color a_l and the region-color s , as in Figure 19, we define

$$(32) \quad z_k^{(0)} := \frac{\det(a_l, p)}{\det(a_l, s)}.$$

Also, if the positive crossing j in Figure 20 (left) is degenerate, then we define

$$(33) \quad \begin{aligned} (w_e^j)^{(0)} &:= \frac{\det(s, p)}{\det(s * a_k, p)}, & (w_f^j)^{(0)} &:= \frac{\det((s * a_l) * a_k, p)}{\det(s * a_k, p)}, \\ (w_g^j)^{(0)} &:= \frac{\det((s * a_l) * a_k, p)}{\det(s * a_l, p)}, & (w_h^j)^{(0)} &:= \frac{\det(s, p)}{\det(s * a_l, p)}, \end{aligned}$$

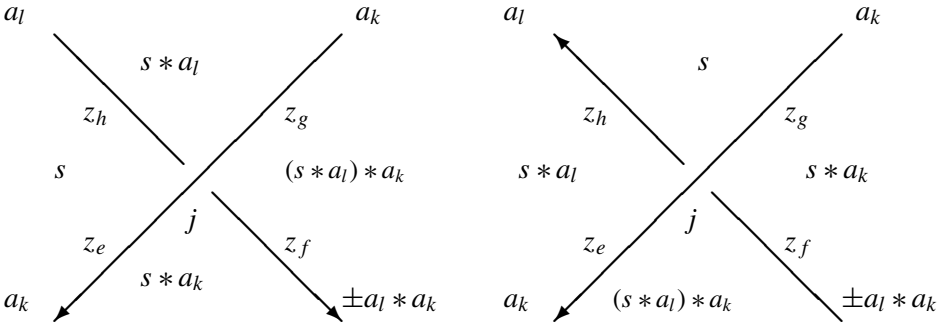


Figure 20. Crossings with shadow-colors and side-variables for a positive crossing (left) and a negative crossing (right).

and, if the negative crossing j in [Figure 20](#) (right) is degenerate, then we define

$$\begin{aligned}
 (w_e^j)^{(0)} &:= \frac{\det(s * a_l, p)}{\det((s * a_l) * a_k, p)}, & (w_f^j)^{(0)} &:= \frac{\det(s * a_k, p)}{\det((s * a_l) * a_k, p)}, \\
 (w_g^j)^{(0)} &:= \frac{\det(s * a_k, p)}{\det(s, p)}, & (w_h^j)^{(0)} &:= \frac{\det(s * a_l, p)}{\det(s, p)}.
 \end{aligned}$$

Then $z_k^{(0)} \neq 0, 1, \infty$, $(w_k^j)^{(0)} \neq 0, 1$ for all possible j, k , and

$$(z_1^{(0)}, \dots, z_n^{(0)}, (w_k^j)^{(0)}, \dots) \in \mathcal{S}.$$

Note that the \pm signs in the arc-colors of [Figure 20](#) appear due to the representatives of the colors in $\mathbb{C}^2 \setminus \{0\}$. However, \pm does not change the value of $z_k^{(0)}$ because

$$\frac{\det(\pm a_l, p)}{\det(\pm a_l, s)} = \frac{\det(a_l, p)}{\det(a_l, s)} = z_k^{(0)}.$$

Likewise, the value of $(w_k^j)^{(0)}$ does not depend on the choice of \pm because the representatives of region-colors are uniquely determined from the fact $s * (\pm a) = s * a$ for any $s, a \in \mathbb{C}^2 \setminus \{0\}$.

Proof of [Theorem 3.2](#). First, when the crossing j in [Figure 20](#) is degenerate, we will show

$$(34) \quad z_e^{(0)} = z_f^{(0)} = z_g^{(0)} = z_h^{(0)},$$

which satisfies [\(31\)](#). Using $h(a_k) = h(a_l)$, we put $a_k = (\alpha \ \beta)$ and $a_l = (c \alpha \ c \ \beta) = c a_k$ for some constant $c \in \mathbb{C} \setminus \{0\}$. Then we obtain $a_l * a_k = a_l$ and, if j is a positive

crossing, then

$$\begin{aligned}
 z_e^{(0)} &= \frac{c \det(a_k, p)}{c \det(a_k, s)} = \frac{\det(a_l, p)}{\det(a_l, s)} = z_h^{(0)}, \\
 z_f^{(0)} &= \frac{\det(\pm a_l * a_k, p)}{\det(\pm a_l * a_k, s * a_k)} = \frac{\det(a_l * a_k, p)}{\det(a_l * a_k, s * a_k)} = \frac{\det(a_l, p)}{\det(a_l, s)} = z_h^{(0)}, \\
 z_g^{(0)} &= \frac{c \det(a_k, p)}{c \det(a_k, s * a_l)} = \frac{\det(a_l, p)}{\det(a_l, s * a_l)} = z_h^{(0)}.
 \end{aligned}$$

If j is a negative crossing, then by exchanging the indices $e \leftrightarrow g$ in the above calculation, we obtain the same result.

Note that [Lemma 2.4](#) and the definition of p in [Section 2C](#) guarantee $z_k^{(0)} \neq 0, 1, \infty$ and $(w_k^j)^{(0)} \neq 0, 1$, so we will concentrate on proving

$$(z_1^{(0)}, \dots, z_n^{(0)}, (w_k^j)^{(0)}, \dots) \in \mathcal{S}.$$

Consider the positive crossing j in [Figure 20](#) (top left) and assume it is nondegenerate. Also consider the tetrahedra in [Figures 9](#) (left) and [10](#) (left), and assign variables z_e, z_f, z_g, z_h to sides of the link diagram as in [Figure 20](#) (top left). Then, using [\(21\)](#) and [\(32\)](#), the shape parameters assigned to the horizontal edges $A_j B_j$ and $D_j A_j$ are

$$\begin{aligned}
 1 &\neq [h(s * a_k), h(p), h(\pm a_l * a_k), h(a_k)] \\
 &= \frac{\det(s, a_k)}{\det(s * a_k, \pm a_l * a_k)} \frac{\det(p, \pm a_l * a_k)}{\det(p, a_k)} = \frac{z_f^{(0)}}{z_e^{(0)}}, \\
 1 &\neq [h(s), h(p), h(a_k), h(a_l)] = \frac{\det(s, a_l)}{\det(s, a_k)} \frac{\det(p, a_k)}{\det(p, a_l)} = \frac{z_e^{(0)}}{z_h^{(0)}},
 \end{aligned}$$

respectively. Likewise, the shape parameters assigned to $B_j C_j$ and $C_j D_j$ are $z_g^{(0)} / z_f^{(0)}$ and $z_h^{(0)} / z_g^{(0)}$ respectively. Furthermore, for any $a, b \in \mathbb{C}^2 \setminus \{0\}$, we can easily show that $h(a * b - a) = h(b)$. If $z_g^{(0)} / z_e^{(0)} = \det(a_k, s) / \det(a_k, s * a_l) = 1$, then $h(a_k) = h(s * a_l - s) = h(a_l)$, which is contradiction. Therefore, we obtain $z_g^{(0)} / z_e^{(0)} \neq 1$, and $z_h^{(0)} / z_f^{(0)} \neq 1$ can be obtained similarly.

We can verify the same holds for nondegenerate negative crossings j in the same way.

Now consider the case when the positive crossing j in [Figure 20](#) (top left) is degenerate. (See [Figures 7](#) (right) and [11](#) (left).) Then, using [\(21\)](#) and [\(33\)](#), the shape parameters assigned to the edges $F_j A_j, E_j B_j, F_j C_j$ and $E_j D_j$ in [Figure 7](#) (right) are

$$\begin{aligned}
 [h(a_k), h(s), h(p), h(s * a_l)] [h(a_k), h(s * a_k), h((s * a_l) * a_k), h(p)] \\
 &= \frac{\det(s, p)}{\det(s * a_k, p)} = (w_e^j)^{(0)}, \\
 [h(\pm a_l * a_k), h(p), h((s * a_l) * a_k), h(s * a_k)] &= \frac{\det(p, (s * a_l) * a_k)}{\det(p, s * a_k)} = (w_f^j)^{(0)},
 \end{aligned}$$

$$[h(a_k), h((s * a_l) * a_k), h(p), h(s * a_k)][h(a_k), h(s * a_l), h(s), h(p)] = \frac{\det((s * a_l) * a_k, p)}{\det(s * a_l, p)} = (w_g^j)^{(0)},$$

$$[h(a_l), h(p), h(s), h(s * a_l)] = \frac{\det(p, s)}{\det(p, s * a_l)} = (w_h^j)^{(0)},$$

respectively. We can verify the same holds for degenerate negative crossings j in the same way.

Therefore $(z_1^{(0)}, \dots, z_n^{(0)}, (w_k^j)^{(0)}, \dots)$ satisfies the hyperbolicity equations of octahedral triangulation defined in Section 2C and, from Proposition 3.1, we get that $(z_1^{(0)}, \dots, z_n^{(0)}, (w_k^j)^{(0)}, \dots)$ is a solution of \mathcal{H} . By the definition of \mathcal{S} , we obtain $(z_1^{(0)}, \dots, z_n^{(0)}, (w_k^j)^{(0)}, \dots) \in \mathcal{S}$. \square

To get the complex volume of ρ from the potential function $V(z_1, \dots, z_n, (w_k^j), \dots)$, we modify it to

$$(35) \quad V_0(z_1, \dots, z_n, (w_k^j), \dots) := V(z_1, \dots, z_n, (w_k^j), \dots) - \sum_k \left(z_k \frac{\partial V}{\partial z_k} \right) \log z_k - \sum_{j:\text{degenerate}} \left(w_k^j \frac{\partial V}{\partial w_k^j} \right) \log w_k^j.$$

This modification guarantees the invariance of the value under the choice of any log-branch. (See Lemma 2.1 of [Cho et al. 2014].) Note that $V_0(z_1^{(0)}, \dots, z_n^{(0)}, (w_k^j)^{(0)}, \dots)$ means the evaluation of the function $V_0(z_1, \dots, z_n, (w_k^j), \dots)$ at

$$(z_1^{(0)}, \dots, z_n^{(0)}, (w_k^j)^{(0)}, \dots).$$

Theorem 3.3. Consider a hyperbolic link L , the shadow-coloring induced by ρ , the potential function $V(z_1, \dots, z_n, (w_k^j), \dots)$ and the solution

$$(z_1^{(0)}, \dots, z_n^{(0)}, (w_k^j)^{(0)}, \dots) \in \mathcal{S}$$

defined in Theorem 3.2. Then,

$$(36) \quad V_0(z_1^{(0)}, \dots, z_n^{(0)}, (w_k^j)^{(0)}, \dots) \equiv i(\text{vol}(\rho) + i \text{cs}(\rho)) \pmod{\pi^2}.$$

Proof. When the crossing j is degenerate, direct calculation shows that the potential function V_j of the crossing defined at (28) satisfies

$$(37) \quad (V_j)_0(z, z, z, z, w_1, w_2, w_3) = 0,$$

for any nonzero values of z, w_1, w_2, w_3 . To simplify the potential function, we rearrange the side variables z_1, \dots, z_n to $z_1, \dots, z_r, z_{r+1}, z_{r+1}^1, z_{r+1}^2, z_{r+1}^3, \dots, z_t, \dots, z_t^3$ so that all endpoints of sides with variables z_1, \dots, z_r are nondegenerate crossings and the degenerate crossings induce $z_{r+1}^{(0)} = (z_{r+1}^1)^{(0)} = (z_{r+1}^2)^{(0)} = (z_{r+1}^3)^{(0)}, \dots, z_t^{(0)} = \dots = (z_t^3)^{(0)}$. (Refer to (34).) Then we define the simplified

potential function \widehat{V} by

$$\widehat{V}(z_1, \dots, z_t) := \sum_{j:\text{nondegenerate}} V_j(z_1, \dots, z_r, z_{r+1}, z_{r+1}, z_{r+1}, z_{r+1}, \dots, z_t, z_t, z_t, z_t).$$

Note that \widehat{V} is obtained from V by removing the potential functions (28) of the degenerate crossings and substituting the side variables z_e, z_f, z_g, z_h around the degenerate crossing with z_e . From (37), we have

$$\widehat{V}_0(z_1^{(0)}, \dots, z_t^{(0)}) = V_0(z_1^{(0)}, \dots, z_n^{(0)}, (w_k^j)^{(0)}, \dots),$$

which suggests \widehat{V} is just a simplification of V with the same value. Therefore, from now on, we will use only \widehat{V} and substitute the side variables of the link diagram $z_{r+1}^1, z_{r+1}^2, z_{r+1}^3$ with z_{r+1} and z_t^1, \dots, z_t^3 with z_t , etc, except at Lemma 3.4 below. Also, we remove octahedra (15) or (16) placed at all degenerate crossings (in other words, the octahedra in Figure 10) because they do not have any effect on the complex volume. (See the comment below the proof of Theorem 2.11.)

Now we will follow ideas of the proof of Theorem 1.2 in [Cho et al. 2014]. However, due to the degenerate crossings, we will improve the proof to cover more general cases. At first, we define r_k by

$$(38) \quad r_k \pi i = z_k \frac{\partial \widehat{V}}{\partial z_k} \Big|_{z_1=z_1^{(0)}, \dots, z_t=z_t^{(0)}},$$

for $k = 1, \dots, t$, where $\Big|_{z_1=z_1^{(0)}, \dots, z_t=z_t^{(0)}}$ means the evaluation of the equation at $(z_1^{(0)}, \dots, z_t^{(0)})$. Unlike [Cho et al. 2014], we cannot guarantee r_k is an even integer yet, so we need the following lemma.

Lemma 3.4. *For the value $z_k^{(0)}$ defined in Theorem 3.2, $(z_1^{(0)}, \dots, z_t^{(0)})$ is a solution of the set of equations*

$$\widehat{\mathcal{H}} = \left\{ \exp\left(z_k \frac{\partial \widehat{V}}{\partial z_k}\right) = 1 \mid k = 1, \dots, t \right\}.$$

Proof. For a degenerate crossing j , from (28),

$$V_j(z_k, z_k, z_k, z_k, w_e^j, w_f^j, w_g^j) = (-\log w_e^j + \log w_f^j - \log w_g^j + \log w_h^j) \log z_k.$$

Therefore, using $w_f^j w_h^j / (w_e^j w_g^j) = 1$, we obtain

$$\exp\left(z_k \frac{\partial V_j}{\partial z_k}(z_k, z_k, z_k, z_k, w_e^j, w_f^j, w_g^j)\right) = 1.$$

This equation implies that, if we substitute the variables $z_{r+1}^1, z_{r+1}^2, z_{r+1}^3$ with z_{r+1} and z_t^1, \dots, z_t^3 with z_t , etc., in the equation of \mathcal{H} , it becomes $\widehat{\mathcal{H}}$. Thus, Theorem 3.2 induces this lemma. □

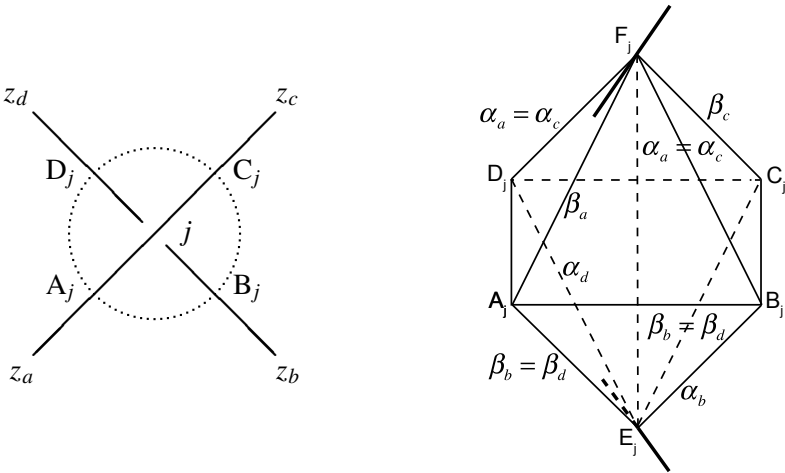


Figure 21. Long-edge parameters of nonhorizontal edges.

As a corollary of Lemma 3.4, now we know r_k defined in (38) is an even integer. To avoid redundant complicated indices, we use z_k instead of $z_k^{(0)}$ in this proof from now on. Using the even integer r_k , we can denote $V_0(z_1, \dots, z_t)$ by

$$(39) \quad \widehat{V}_0(z_1, \dots, z_t) = \widehat{V}(z_1, \dots, z_t) - \sum_{k=1}^t r_k \pi i \log z_k.$$

Now we introduce notations $\alpha_m, \beta_m, \gamma_l, \delta_j$ for the long-edge parameters defined in (20). We assign α_m and β_m to nonhorizontal edges as in Figure 21, where m is over all sides of the link diagram. (Recall that the edges A_jB_j, B_jC_j, C_jD_j and D_jA_j in Figure 21 were named horizontal edges.) We also assign γ_l to horizontal edges, where l is over all regions, and δ_j to the edge E_jF_j inside the octahedron. Although we have $\alpha_a = \alpha_c$ and $\beta_b = \beta_d$ because of the gluing, we use α_a for the tetrahedra $E_jF_jA_jB_j$ and $E_jF_jA_jD_j$, α_c for $E_jF_jC_jB_j$ and $E_jF_jC_jD_j$, β_b for $E_jF_jA_jB_j$ and $E_jF_jC_jB_j$, and β_d for $E_jF_jC_jD_j$ and $E_jF_jA_jD_j$. Note that the labeling is consistent even when some crossing is degenerate because, when the crossing j in Figure 21 is degenerate, we obtain $z_a = z_b = z_c = z_d$ and, after removing the octahedron of the crossing, the long-edge parameters satisfy $\alpha_a = \alpha_b = \alpha_c = \alpha_d$ and $\beta_a = \beta_b = \beta_c = \beta_d$.

Now consider a side with variable z_k and two possible cases in Figure 22. We consider the case when the crossing is nondegenerate, or equivalently, $z_a \neq z_k \neq z_b$. (If it is degenerate, we assume there is a degenerated octahedron⁹ at the crossing.) For $m = a, b$, let $\sigma_k^m \in \{\pm 1\}$ be the sign of the tetrahedron¹⁰ between the sides z_k and z_m , and u_k^m be the shape parameter of the tetrahedron assigned to the horizontal edge. We put $\tau_k^m = 1$ when z_k is the numerator of $(u_k^m)^{\sigma_k^m}$ and $\tau_k^m = -1$ otherwise. We also

⁹ An octahedron is called degenerate when two vertices at the top and the bottom coincide.

¹⁰ The sign of a tetrahedron is the sign of the coordinate in (13) or (14).

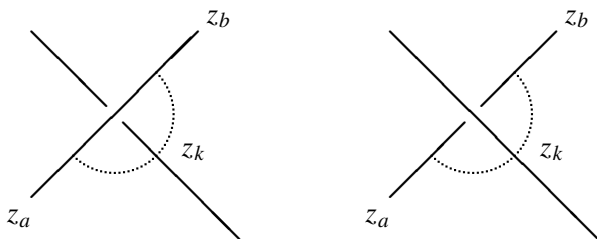


Figure 22. Two cases with respect to z_k .

define p_k^m and q_k^m by (25) so that $\sigma_k^m[(u_k^m)^{\sigma_k^m}; p_k^m, q_k^m]$ becomes the element of $\widehat{\mathcal{P}}(\mathbb{C})$ corresponding to the tetrahedron. Then $\frac{1}{2} \sum_{1 \leq k, m \leq t} \sigma_k^m[(u_k^m)^{\sigma_k^m}; p_k^m, q_k^m]$ is the element¹¹ of $\widehat{\mathcal{B}}(\mathbb{C})$ corresponding to the octahedral triangulation in Section 2C, and

$$(40) \quad \frac{1}{2} \sum_{1 \leq k, m \leq t} \sigma_k^m \widehat{L}[(u_k^m)^{\sigma_k^m}; p_k^m, q_k^m] \equiv i(\text{vol}(\rho) + i \text{cs}(\rho)) \pmod{\pi^2},$$

from Theorem 2.11.

By definition, we know

$$(41) \quad u_k^a = \frac{z_k}{z_a}, \quad u_k^b = \frac{z_b}{z_k}.$$

In the case of Figure 22 (left), we have

$$\sigma_k^a = 1, \sigma_k^b = -1 \quad \text{and} \quad \tau_k^a = \tau_k^b = 1.$$

Using (25) and Figure 23 (left), we decide p_k^m and q_k^m as follows:

$$(42) \quad \begin{cases} \log(z_k/z_a) + p_k^a \pi i = (\log \alpha_k - \log \beta_k) - (\log \alpha_a - \log \beta_a), \\ \log(z_k/z_b) + p_k^b \pi i = (\log \alpha_k - \log \beta_k) - (\log \alpha_b - \log \beta_b), \end{cases}$$

$$(43) \quad \begin{cases} -\log(1 - z_k/z_a) + q_k^a \pi i = \log \beta_k + \log \alpha_a - \log \gamma_1 - \log \delta_1, \\ -\log(1 - z_k/z_b) + q_k^b \pi i = \log \beta_k + \log \alpha_b - \log \gamma_2 - \log \delta_1. \end{cases}$$

In the case of Figure 22 (right), we have

$$\sigma_k^a = -1, \sigma_k^b = 1 \quad \text{and} \quad \tau_k^a = \tau_k^b = -1.$$

Using (25) and Figure 23 (right), we decide p_k^m and q_k^m as follows:

$$(44) \quad \begin{cases} \log(z_a/z_k) + p_k^a \pi i = (\log \alpha_a - \log \beta_a) - (\log \alpha_k - \log \beta_k), \\ \log(z_b/z_k) + p_k^b \pi i = (\log \alpha_b - \log \beta_b) - (\log \alpha_k - \log \beta_k), \end{cases}$$

¹¹ The coefficient $\frac{1}{2}$ appears because the same tetrahedron is counted twice in the summation.

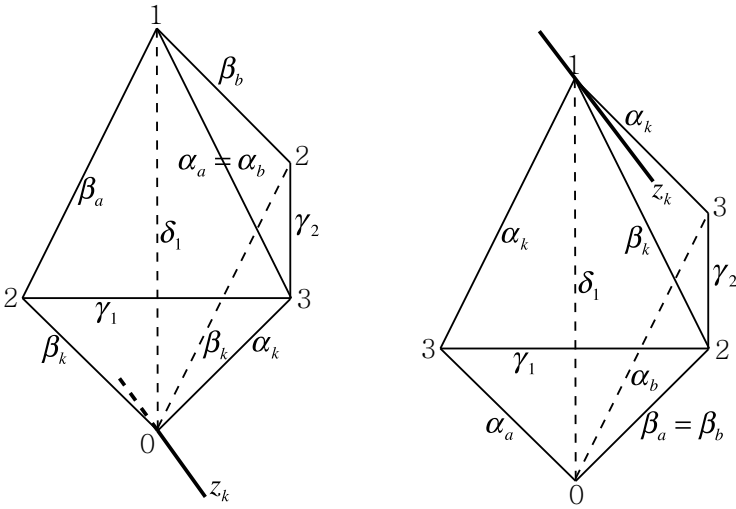


Figure 23. Tetrahedra of Figure 22.

$$(45) \quad \begin{cases} -\log(1 - z_a/z_k) + q_k^a \pi i = \log \beta_a + \log \alpha_k - \log \gamma_1 - \log \delta_1, \\ -\log(1 - z_b/z_k) + q_k^b \pi i = \log \beta_b + \log \alpha_k - \log \gamma_2 - \log \delta_1. \end{cases}$$

The equations (42) and (44) hold for all (nondegenerate and degenerate) crossings, so we get the following observation.

Observation 3.5. We have

$$\log \alpha_k - \log \beta_k \equiv \log z_k + A \pmod{\pi i},$$

for all $k = 1, \dots, t$, where A is a complex constant number independent of k .

Note that, by (27), the potential function \widehat{V} is expressed by

$$(46) \quad \widehat{V}(z_1, \dots, z_t) = \frac{1}{2} \sum_{1 \leq k, m \leq t} \sigma_k^m \text{Li}_2((u_k^m)^{\sigma_k^m}) = \frac{1}{2} \sum_{k=1}^t \sum_{m=a, \dots, d} \sigma_k^m \text{Li}_2((u_k^m)^{\sigma_k^m}),$$

where the range of the index m is determined by k and we define the range of m by $m = a, \dots, d$ ¹² from now on. Recall that r_k was defined in (38). Direct calculation shows

$$r_k \pi i = - \sum_{m=a, \dots, d} \sigma_k^m \tau_k^m \log(1 - (u_k^m)^{\sigma_k^m}).$$

Combining (43) and (45), we obtain

$$\sum_{m=a, b} \sigma_k^m \tau_k^m \left\{ -\log(1 - (u_k^m)^{\sigma_k^m}) + q_k^m \pi i \right\} = -\log \gamma_1 + \log \gamma_2,$$

¹² The range $m = a, \dots, d$ means that each side with one of the side variables z_a, \dots, z_d shares a nondegenerate crossing with a side with z_k .

for both cases in Figure 22. (Note that $\alpha_a = \alpha_b$ in (43) and $\beta_a = \beta_b$ in (45).) Therefore, we obtain

$$\sum_{m=a,\dots,d} \sigma_k^m \tau_k^m \left\{ -\log(1 - (u_k^m)^{\sigma_k^m}) + q_k^m \pi i \right\} = 0,$$

and

$$(47) \quad r_k \pi i = - \sum_{m=a,\dots,d} \sigma_k^m \tau_k^m q_k^m \pi i.$$

Lemma 3.6. *For all possible k and m , we have*

$$(48) \quad \frac{1}{2} \sum_{1 \leq k, m \leq t} \sigma_k^m q_k^m \pi i \log(u_k^m)^{\sigma_k^m} \equiv - \sum_{k=1}^t r_k \pi i \log z_k \pmod{2\pi^2}.$$

Proof. Note that, by definition, $\sigma_k^m = \sigma_m^k$, $\tau_k^m = -\tau_m^k$ and

$$(u_k^m)^{\sigma_k^m} = \left(\frac{z_k}{z_m} \right)^{\tau_k^m} = (z_k)^{\tau_k^m} (z_m)^{-\tau_k^m}.$$

Using the above and (47), we can directly calculate

$$\begin{aligned} \frac{1}{2} \sum_{k=1}^t \sum_{m=a,\dots,d} \sigma_k^m q_k^m \pi i \log(u_k^m)^{\sigma_k^m} &\equiv \sum_{k=1}^t \left(\sum_{m=a,\dots,d} \sigma_k^m \tau_k^m q_k^m \pi i \right) \log z_k \pmod{2\pi^2} \\ &= - \sum_{k=1}^t r_k \pi i \log z_k. \quad \square \end{aligned}$$

Lemma 3.7. *For all possible k and m , we have*

$$\frac{1}{2} \sum_{1 \leq k, m \leq t} \sigma_k^m \log(1 - (u_k^m)^{\sigma_k^m}) (\log(u_k^m)^{\sigma_k^m} + p_k^m \pi i) \equiv - \sum_{k=1}^t r_k \pi i \log z_k \pmod{2\pi^2}.$$

Proof. From (42) and (44), we have

$$\log(u_k^m)^{\sigma_k^m} + p_k^m \pi i = \tau_k^m (\log \alpha_k - \log \beta_k) + \tau_m^k (\log \alpha_m - \log \beta_m).$$

Therefore,

$$\begin{aligned} \frac{1}{2} \sum_{1 \leq k, m \leq t} \sigma_k^m \log(1 - (u_k^m)^{\sigma_k^m}) (\log(u_k^m)^{\sigma_k^m} + p_k^m \pi i) \\ = \sum_{k=1}^t \left(\sum_{m=a,\dots,d} \sigma_k^m \tau_k^m \log(1 - (u_k^m)^{\sigma_k^m}) \right) (\log \alpha_k - \log \beta_k) \\ = - \sum_{k=1}^t r_k \pi i (\log \alpha_k - \log \beta_k). \end{aligned}$$

Note that

$$\sum_{k=1}^t r_k \pi i = \sum_{k=1}^t z_k \frac{\partial \widehat{V}}{\partial z_k} = 0$$

because \widehat{V} is expressed by the summation of certain forms of $\text{Li}_2(z_a/z_b)$ and

$$z_a \frac{\partial \text{Li}_2(z_a/z_b)}{\partial z_a} + z_b \frac{\partial \text{Li}_2(z_a/z_b)}{\partial z_b} = -\log\left(1 - \frac{z_a}{z_b}\right) + \log\left(1 - \frac{z_a}{z_b}\right) = 0.$$

By using [Observation 3.5](#), the above, and the fact that r_k is even, we have

$$\begin{aligned} -\sum_{k=1}^t r_k \pi i (\log \alpha_k - \log \beta_k) &\equiv -\sum_{k=1}^t r_k \pi i (\log z_k + A) \\ &= -\sum_{k=1}^t r_k \pi i \log z_k \pmod{2\pi^2}. \end{aligned} \quad \square$$

Combining [\(40\)](#), [\(46\)](#), [Lemma 3.6](#) and [Lemma 3.7](#), we complete the proof of [Theorem 3.3](#) as follows:

$$\begin{aligned} &i(\text{vol}(\rho) + i \text{cs}(\rho)) \\ &\equiv \frac{1}{2} \sum_{1 \leq k, m \leq t} \sigma_k^m \widehat{L}[(u_k^m)^{\sigma_k^m}; p_k^m, q_k^m] \\ &= \frac{1}{2} \sum_{1 \leq k, m \leq t} \sigma_k^m \left(\text{Li}_2((u_k^m)^{\sigma_k^m}) - \frac{\pi^2}{6} \right) + \frac{1}{4} \sum_{1 \leq k, m \leq t} \sigma_k^m q_k^m \pi i \log(u_k^m)^{\sigma_k^m} \\ &\quad + \frac{1}{4} \sum_{1 \leq k, m \leq t} \sigma_k^m \log(1 - (u_k^m)^{\sigma_k^m}) (\log(u_k^m)^{\sigma_k^m} + p_k^m \pi i) \\ &\equiv \widehat{V}(z_1, \dots, z_n) - \sum_{k=1}^t r_k \pi i \log z_k = \widehat{V}_0(z_1, \dots, z_t) \pmod{\pi^2}. \end{aligned} \quad \square$$

4. Examples

4A. A figure-eight knot 4₁. For the figure-eight knot diagram in [Figure 24](#), let the elements of \mathcal{P} corresponding to the arcs be

$$a_1 = (0 \ t), \quad a_2 = (1 \ 0), \quad a_3 = (-t \ 1+t), \quad a_4 = (-t \ t),$$

where t is a solution of $t^2 + t + 1 = 0$. These elements satisfy

$$(49) \quad a_1 * a_2 = a_4, \quad a_3 * a_4 = a_2, \quad a_1 * a_3 = -a_2, \quad a_3 * a_1 = a_4,$$

where the identities are expressed in $\mathbb{C}^2 \setminus \{0\}$, not in $\mathcal{P} = (\mathbb{C}^2 \setminus \{0\})/\pm$. Let $\rho : \pi_1(4_1) \rightarrow \text{PSL}(2, \mathbb{C})$ be the boundary-parabolic representation determined by a_1, \dots, a_4 . We define the shadow-coloring of [Figure 24](#) induced by ρ by letting

$$\begin{aligned} s_1 &= (1 \ 1), & s_2 &= (0 \ 1), & s_3 &= (-t - 1 \ t + 2), \\ s_4 &= (-2t - 1 \ 2t + 3), & s_5 &= (-2t - 1 \ t + 4), & s_6 &= (1 \ t + 2), \end{aligned}$$

and $p = (2 \ 1)$. Direct calculation shows this shadow-coloring satisfies [\(5\)](#) in [Lemma 2.4](#). (However, this does not satisfy [\(6\)](#).)

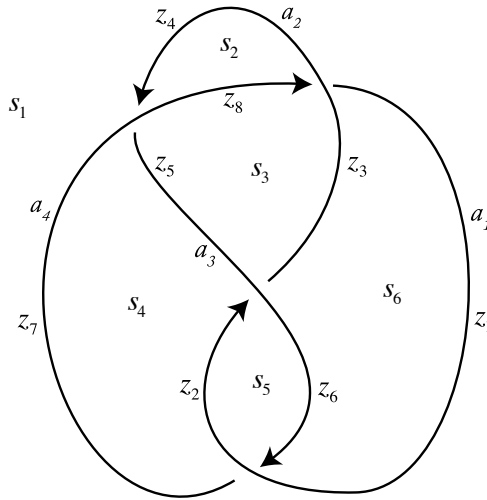


Figure 24. A figure-eight knot 4_1 with parameters.

All values of $h(a_1), \dots, h(a_4)$ are different, therefore the potential function $V(z_1, \dots, z_8)$ of Figure 24 is (29). Applying Theorem 3.2, we obtain

$$\begin{aligned} z_1^{(0)} &= \frac{\det(a_1, p)}{\det(a_1, s_6)} = 2, & z_2^{(0)} &= \frac{\det(a_1, p)}{\det(a_1, s_5)} = \frac{-2}{2t + 1}, \\ z_3^{(0)} &= \frac{\det(a_2, p)}{\det(a_2, s_6)} = \frac{1}{t + 2}, & z_4^{(0)} &= \frac{\det(a_2, p)}{\det(a_2, s_1)} = 1, \\ z_5^{(0)} &= \frac{\det(a_3, p)}{\det(a_3, s_4)} = -3t - 2, & z_6^{(0)} &= \frac{\det(a_3, p)}{\det(a_3, s_5)} = \frac{3t + 2}{2t}, \\ z_7^{(0)} &= \frac{\det(a_4, p)}{\det(a_4, s_4)} = \frac{3}{2}, & z_8^{(0)} &= \frac{\det(a_4, p)}{\det(a_4, s_3)} = 3, \end{aligned}$$

and $(z_1^{(0)}, \dots, z_8^{(0)})$ becomes a solution of $\mathcal{H} = \{\exp(z_k \frac{\partial V}{\partial z_k}) = 1 \mid k = 1, \dots, 8\}$. Applying Theorem 3.3, we obtain

$$V_0(z_1^{(0)}, \dots, z_8^{(0)}) \equiv i(\text{vol}(\rho) + i \text{cs}(\rho)) \pmod{\pi^2},$$

and numerical calculation verifies it by

$$V_0(z_1^{(0)}, \dots, z_8^{(0)}) = \begin{cases} i(2.0299\dots + 0i) = i(\text{vol}(4_1) + i \text{cs}(4_1)) & \text{if } t = \frac{1}{2}(-1 - \sqrt{3}i), \\ i(-2.0299\dots + 0i) = i(-\text{vol}(4_1) + i \text{cs}(4_1)) & \text{if } t = \frac{1}{2}(-1 + \sqrt{3}i). \end{cases}$$

4B. Trefoil knot 3_1 . For the trefoil knot diagram in Figure 25, let the elements of \mathcal{P} corresponding to the arcs be

$$a_1 = (1 \ 0), \quad a_2 = (0 \ 1), \quad a_3 = a_4 = (-1 \ 1).$$

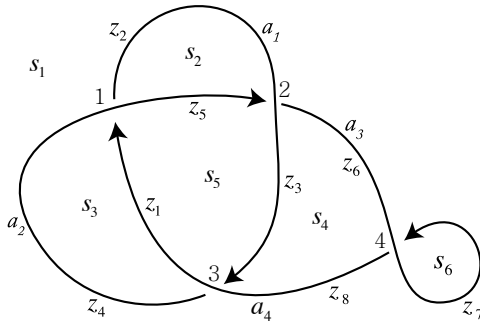


Figure 25. A trefoil knot 3_1 with parameters.

(Note that crossing 4 is degenerate.) These elements satisfy

$$(50) \quad a_1 * a_2 = -a_1, \quad a_2 * a_1 = a_3, \quad a_1 * a_4 = a_2, \quad a_4 * a_3 = a_3,$$

where the identities are expressed in $\mathbb{C}^2 \setminus \{0\}$, not in $\mathcal{P} = (\mathbb{C}^2 \setminus \{0\})/\pm$. Let $\rho : \pi_1(3_1) \rightarrow \text{PSL}(2, \mathbb{C})$ be the boundary-parabolic representation determined by a_1, a_2, a_3, a_4 . We define the shadow-coloring of Figure 24 induced by ρ by letting

$$\begin{aligned} s_1 &= \begin{pmatrix} -1 & 2 \\ 0 & 1 \end{pmatrix}, & s_2 &= \begin{pmatrix} 1 & 2 \\ 0 & 1 \end{pmatrix}, & s_3 &= \begin{pmatrix} -1 & 3 \\ 0 & 1 \end{pmatrix}, \\ s_4 &= \begin{pmatrix} 0 & 1 \\ 0 & 1 \end{pmatrix}, & s_5 &= \begin{pmatrix} 1 & 1 \\ 0 & 1 \end{pmatrix}, & s_6 &= \begin{pmatrix} -2 & 3 \\ 0 & 1 \end{pmatrix}, \end{aligned}$$

and $p = \begin{pmatrix} 2 & 1 \\ 0 & 1 \end{pmatrix}$. Direct calculation shows this shadow-coloring satisfies (5) in Lemma 2.4. (However, this does not satisfy (6).)

All values of $h(a_1), h(a_2), h(a_3) = h(a_4)$ are different, hence the potential function V of Figure 25 is

$$\begin{aligned} V(z_1, \dots, z_8, w_6^4, w_7^4) &= \text{Li}_2\left(\frac{z_2}{z_5}\right) - \text{Li}_2\left(\frac{z_2}{z_4}\right) + \text{Li}_2\left(\frac{z_1}{z_4}\right) - \text{Li}_2\left(\frac{z_1}{z_5}\right) \\ &\quad + \text{Li}_2\left(\frac{z_6}{z_3}\right) - \text{Li}_2\left(\frac{z_6}{z_2}\right) + \text{Li}_2\left(\frac{z_5}{z_2}\right) - \text{Li}_2\left(\frac{z_5}{z_3}\right) \\ &\quad + \text{Li}_2\left(\frac{z_4}{z_1}\right) - \text{Li}_2\left(\frac{z_4}{z_8}\right) + \text{Li}_2\left(\frac{z_3}{z_8}\right) - \text{Li}_2\left(\frac{z_3}{z_1}\right) \\ &\quad - \log w_6^4 \log z_6 + \log w_7^4 \log z_8, \end{aligned}$$

and the simplified potential function \widehat{V} defined in the proof of Theorem 3.3 is

$$\begin{aligned} \widehat{V}(z_1, \dots, z_6) &= \text{Li}_2\left(\frac{z_2}{z_5}\right) - \text{Li}_2\left(\frac{z_2}{z_4}\right) + \text{Li}_2\left(\frac{z_1}{z_4}\right) - \text{Li}_2\left(\frac{z_1}{z_5}\right) \\ &\quad + \text{Li}_2\left(\frac{z_6}{z_3}\right) - \text{Li}_2\left(\frac{z_6}{z_2}\right) + \text{Li}_2\left(\frac{z_5}{z_2}\right) - \text{Li}_2\left(\frac{z_5}{z_3}\right) \\ &\quad + \text{Li}_2\left(\frac{z_4}{z_1}\right) - \text{Li}_2\left(\frac{z_4}{z_6}\right) + \text{Li}_2\left(\frac{z_3}{z_6}\right) - \text{Li}_2\left(\frac{z_3}{z_1}\right). \end{aligned}$$

Applying [Theorem 3.2](#), we obtain

$$\begin{aligned} z_1^{(0)} &= \frac{\det(a_4, p)}{\det(a_4, s_5)} = \frac{3}{2}, & z_2^{(0)} &= \frac{\det(a_1, p)}{\det(a_1, s_2)} = \frac{1}{2}, \\ z_3^{(0)} &= \frac{\det(a_1, p)}{\det(a_1, s_5)} = 1, & z_4^{(0)} &= \frac{\det(a_2, p)}{\det(a_2, s_3)} = -2, \\ z_5^{(0)} &= \frac{\det(a_2, p)}{\det(a_2, s_5)} = 2, & z_6^{(0)} = z_7^{(0)} = z_8^{(0)} &= \frac{\det(a_3, p)}{\det(a_3, s_4)} = 3, \\ (w_6^4)^{(0)} &= \frac{\det(s_1, p)}{\det(s_4, p)} = \frac{5}{2}, & (w_7^4)^{(0)} &= \frac{\det(s_1, p)}{\det(s_6, p)} = \frac{5}{8}. \end{aligned}$$

Note that $(z_1^{(0)}, \dots, z_8^{(0)}, (w_6^4)^{(0)}, (w_7^4)^{(0)})$ and $(z_1^{(0)}, \dots, z_6^{(0)})$ are solutions of

$$\mathcal{H} = \left\{ \exp\left(z_k \frac{\partial V}{\partial z_k}\right) = 1, \exp\left(w_k^j \frac{\partial V}{\partial w_k^j}\right) = 1 \mid j = 4, k = 1, \dots, 8 \right\}$$

and $\widehat{\mathcal{H}} = \left\{ \exp\left(z_k \frac{\partial \widehat{V}}{\partial z_k}\right) = 1 \mid k = 1, \dots, 6 \right\},$

respectively. Applying [Theorem 3.3](#), we obtain

$$V_0(z_1^{(0)}, \dots, (w_7^4)^{(0)}) \equiv \widehat{V}_0(z_1^{(0)}, \dots, z_6^{(0)}) \equiv i(\text{vol}(\rho) + i \text{cs}(\rho)) \pmod{\pi^2},$$

and numerical calculation verifies it by

$$\widehat{V}_0(z_1^{(0)}, \dots, z_6^{(0)}) = i(0 + 1.6449\dots i),$$

where $\text{vol}(3_1) = 0$ holds trivially and $1.6449\dots = \pi^2/6$ holds numerically.

Acknowledgements

The author thanks Yuichi Kabaya and Jun Murakami for suggesting this research and having much discussion. Ayumu Inoue gave wonderful lectures on his work [\[Inoue and Kabaya 2014\]](#) at Seoul National University and it became the framework for [Section 2](#) of this article. Many people, including Hyuk Kim, Seonhwa Kim, Roland van der Veen, Hitoshi Murakami, Satoshi Nawata, and Stephané Baseilhac heard my talks on the result and gave many suggestions. Special thanks are due to the reviewer who suggested the revised proof of [Lemma 2.4](#).

The author is supported by the Basic Science Research Program through the National Research Foundation of Korea (NRF) funded by the Ministry of Education (NRF-2015R1C1A1A02037540).

References

[Baseilhac and Benedetti 2007] S. Baseilhac and R. Benedetti, “Quantum hyperbolic geometry”, *Algebr. Geom. Topol.* **7** (2007), 845–917. [MR Zbl](#)

- [Cho 2016a] J. Cho, “Optimistic limit of the colored Jones polynomial and the existence of a solution”, *Proc. Amer. Math. Soc.* **144**:4 (2016), 1803–1814. [MR](#) [Zbl](#)
- [Cho 2016b] J. Cho, “Optimistic limits of the colored Jones polynomials and the complex volumes of hyperbolic links”, *J. Aust. Math. Soc.* **100**:3 (2016), 303–337. [MR](#) [Zbl](#)
- [Cho and Murakami 2017] J. Cho and J. Murakami, “Reidemeister transformations of the potential function and the solution”, *J. Knot Theory Ramifications* **26**:12 (2017), art. id. 1750079. [MR](#) [Zbl](#)
- [Cho et al. 2014] J. Cho, H. Kim, and S. Kim, “Optimistic limits of Kashaev invariants and complex volumes of hyperbolic links”, *J. Knot Theory Ramifications* **23**:9 (2014), art. id. 1450049. [MR](#) [Zbl](#)
- [Elhamdadi and Nelson 2015] M. Elhamdadi and S. Nelson, *Quandles: an introduction to the algebra of knots*, Student Mathematical Library **74**, Amer. Math. Soc., Providence, RI, 2015. [MR](#) [Zbl](#)
- [Garoufalidis et al. 2015] S. Garoufalidis, M. Goerner, and C. K. Zickert, “The Ptolemy field of 3-manifold representations”, *Algebr. Geom. Topol.* **15**:1 (2015), 371–397. [MR](#) [Zbl](#)
- [Hikami and Inoue 2015] K. Hikami and R. Inoue, “Braids, complex volume and cluster algebras”, *Algebr. Geom. Topol.* **15**:4 (2015), 2175–2194. [MR](#) [Zbl](#)
- [Inoue and Kabaya 2014] A. Inoue and Y. Kabaya, “Quandle homology and complex volume”, *Geom. Dedicata* **171** (2014), 265–292. [MR](#) [Zbl](#)
- [Kashaev 1995] R. M. Kashaev, “A link invariant from quantum dilogarithm”, *Modern Phys. Lett. A* **10**:19 (1995), 1409–1418. [MR](#) [Zbl](#)
- [Murakami 2000] H. Murakami, “The asymptotic behavior of the colored Jones function of a knot and its volume”, preprint, 2000. [arXiv](#)
- [Neumann 2004] W. D. Neumann, “Extended Bloch group and the Cheeger–Chern–Simons class”, *Geom. Topol.* **8** (2004), 413–474. [MR](#) [Zbl](#)
- [Neumann and Yang 1999] W. D. Neumann and J. Yang, “Bloch invariants of hyperbolic 3-manifolds”, *Duke Math. J.* **96**:1 (1999), 29–59. [MR](#) [Zbl](#)
- [Rolfsen 1976] D. Rolfsen, *Knots and links*, Mathematics Lecture Series **7**, Publish or Perish, Berkeley, CA, 1976. [MR](#) [Zbl](#)
- [Sakuma and Yokota 2016] M. Sakuma and Y. Yokota, “An application of non-positively curved cubings of alternating links”, preprint, 2016. [arXiv](#)
- [Thurston 1999] D. Thurston, “Hyperbolic volume and the Jones polynomial”, lecture notes, 1999, Available at <http://pages.iu.edu/~dpthurst/speaking/Grenoble.pdf>.
- [Weeks 2005] J. Weeks, “Computation of hyperbolic structures in knot theory”, pp. 461–480 in *Handbook of knot theory*, edited by W. Menasco and M. Thistlethwaite, Elsevier, Amsterdam, 2005. [MR](#) [Zbl](#)
- [Yokota 2011] Y. Yokota, “On the complex volume of hyperbolic knots”, *J. Knot Theory Ramifications* **20**:7 (2011), 955–976. [MR](#) [Zbl](#)
- [Zickert 2009] C. K. Zickert, “The volume and Chern–Simons invariant of a representation”, *Duke Math. J.* **150**:3 (2009), 489–532. [MR](#) [Zbl](#)

Received January 16, 2016. Revised January 30, 2018.

JINSEOK CHO
 BUSAN NATIONAL UNIVERSITY OF EDUCATION
 BUSAN
 SOUTH KOREA

dol0425@bnue.ac.kr

PACIFIC JOURNAL OF MATHEMATICS

Founded in 1951 by E. F. Beckenbach (1906–1982) and F. Wolf (1904–1989)

msp.org/pjm

EDITORS

Don Blasius (Managing Editor)
Department of Mathematics
University of California
Los Angeles, CA 90095-1555
blasius@math.ucla.edu

Paul Balmer
Department of Mathematics
University of California
Los Angeles, CA 90095-1555
balmer@math.ucla.edu

Wee Teck Gan
Mathematics Department
National University of Singapore
Singapore 119076
matgwt@nus.edu.sg

Sorin Popa
Department of Mathematics
University of California
Los Angeles, CA 90095-1555
popa@math.ucla.edu

Vyjayanthi Chari
Department of Mathematics
University of California
Riverside, CA 92521-0135
chari@math.ucr.edu

Kefeng Liu
Department of Mathematics
University of California
Los Angeles, CA 90095-1555
liu@math.ucla.edu

Jie Qing
Department of Mathematics
University of California
Santa Cruz, CA 95064
qing@cats.ucsc.edu

Daryl Cooper
Department of Mathematics
University of California
Santa Barbara, CA 93106-3080
cooper@math.ucsb.edu

Jiang-Hua Lu
Department of Mathematics
The University of Hong Kong
Pokfulam Rd., Hong Kong
jhlu@maths.hku.hk

Paul Yang
Department of Mathematics
Princeton University
Princeton NJ 08544-1000
yang@math.princeton.edu

PRODUCTION

Silvio Levy, Scientific Editor, production@msp.org

SUPPORTING INSTITUTIONS

ACADEMIA SINICA, TAIPEI
CALIFORNIA INST. OF TECHNOLOGY
INST. DE MATEMÁTICA PURA E APLICADA
KEIO UNIVERSITY
MATH. SCIENCES RESEARCH INSTITUTE
NEW MEXICO STATE UNIV.
OREGON STATE UNIV.

STANFORD UNIVERSITY
UNIV. OF BRITISH COLUMBIA
UNIV. OF CALIFORNIA, BERKELEY
UNIV. OF CALIFORNIA, DAVIS
UNIV. OF CALIFORNIA, LOS ANGELES
UNIV. OF CALIFORNIA, RIVERSIDE
UNIV. OF CALIFORNIA, SAN DIEGO
UNIV. OF CALIF., SANTA BARBARA

UNIV. OF CALIF., SANTA CRUZ
UNIV. OF MONTANA
UNIV. OF OREGON
UNIV. OF SOUTHERN CALIFORNIA
UNIV. OF UTAH
UNIV. OF WASHINGTON
WASHINGTON STATE UNIVERSITY

These supporting institutions contribute to the cost of publication of this Journal, but they are not owners or publishers and have no responsibility for its contents or policies.


See inside back cover or msp.org/pjm for submission instructions.

The subscription price for 2018 is US \$475/year for the electronic version, and \$640/year for print and electronic. Subscriptions, requests for back issues and changes of subscriber address should be sent to Pacific Journal of Mathematics, P.O. Box 4163, Berkeley, CA 94704-0163, U.S.A. The Pacific Journal of Mathematics is indexed by [Mathematical Reviews](#), [Zentralblatt MATH](#), [PASCAL CNRS Index](#), [Referativnyi Zhurnal](#), [Current Mathematical Publications](#) and [Web of Knowledge \(Science Citation Index\)](#).

The Pacific Journal of Mathematics (ISSN 0030-8730) at the University of California, c/o Department of Mathematics, 798 Evans Hall #3840, Berkeley, CA 94720-3840, is published twelve times a year. Periodical rate postage paid at Berkeley, CA 94704, and additional mailing offices. POSTMASTER: send address changes to Pacific Journal of Mathematics, P.O. Box 4163, Berkeley, CA 94704-0163.

PJM peer review and production are managed by EditFLOW® from Mathematical Sciences Publishers.

PUBLISHED BY

 **mathematical sciences publishers**
nonprofit scientific publishing

<http://msp.org/>

© 2018 Mathematical Sciences Publishers

PACIFIC JOURNAL OF MATHEMATICS

Volume 295 No. 2 August 2018

Nonsmooth convex caustics for Birkhoff billiards	257
MAXIM ARNOLD and MISHA BIALY	
Certain character sums and hypergeometric series	271
RUPAM BARMAN and NEELAM SAIKIA	
On the structure of holomorphic isometric embeddings of complex unit balls into bounded symmetric domains	291
SHAN TAI CHAN	
Hamiltonian stationary cones with isotropic links	317
JINGYI CHEN and YU YUAN	
Quandle theory and the optimistic limits of the representations of link groups	329
JINSEOK CHO	
Classification of positive smooth solutions to third-order PDEs involving fractional Laplacians	367
WEI DAI and GUOLIN QIN	
The projective linear supergroup and the SUSY-preserving automorphisms of $\mathbb{P}^{1 1}$	385
RITA FIORESI and STEPHEN D. KWOK	
The Gromov width of coadjoint orbits of the symplectic group	403
IVA HALACHEVA and MILENA PABINIAK	
Minimal braid representatives of quasipositive links	421
KYLE HAYDEN	
Four-dimensional static and related critical spaces with harmonic curvature	429
JONGSU KIM and JINWOO SHIN	
Boundary Schwarz lemma for nonequidimensional holomorphic mappings and its application	463
YANG LIU, ZHIHUA CHEN and YIFEI PAN	
Theta correspondence and the Prasad conjecture for $SL(2)$	477
HENGFEI LU	
Convexity of level sets and a two-point function	499
BEN WEINKOVE	